

Image Cover Sheet

CLASSIFICATION

UNCLASSIFIED

SYSTEM NUMBER

512408



TITLE

Investigation of Plastic Zone Development in Dynamic Tear Test Specimens

System Number:

Patron Number:

Requester:

Notes:

DSIS Use only:

Deliver to:



INVESTIGATION OF PLASTIC ZONE DEVELOPMENT IN DYNAMIC TEAR TEST SPECIMENS

T.S. Koko – B.K. Gallant – S.M. Tobin

MARTEC Ltd

DEFENCE RESEARCH ESTABLISHMENT ATLANTIC

Contractor Report

DREA CR 1999-095

July 1999



National
Defence

Défense
nationale

Canada



National Defence
Research and
Development Branch

Défense nationale
Bureau de recherche
et développement

DREA CR 1999-095

INVESTIGATION OF PLASTIC ZONE DEVELOPMENT IN DYNAMIC TEAR TEST SPECIMENS

T.S. Koko B.K. Gallant S.M. Tobin

MARTEC Ltd.
400-1888 Brunswick Street
Halifax Nova Scotia Canada
B3J 3J8

Scientific Authority


J.R. Matthews

W7707-8-6180/A
Contract Number

July 1999

CONTRACTOR REPORT

Prepared for

Defence
Research
Establishment
Atlantic



Centre de
Recherches pour la
Défense
Atlantique

Canada

REPRODUCTION QUALITY NOTICE

This document is the best quality available. The copy furnished to DRDCIM contained pages that may have the following quality problems:

- : Pages smaller or Larger than normal**
- : Pages with background colour or light coloured printing**
- : Pages with small type or poor printing; and or**
- : Pages with continuous tone material or colour photographs**

Due to various output media available these conditions may or may not cause poor legibility in the hardcopy output you receive.

☒ **If this block is checked, the copy furnished to DRDCIM contained pages with colour printing, that when reproduced in Black and White, may change detail of the original copy.**

ABSTRACT

The J-Integral is an elastic-plastic fracture criterion, which permits measurement of the fracture toughness of a specimen that has been fractured after general yielding. However, an understanding of the ratio of plastic zone size (radius) to the crack tip blunting (stretch zone) required to determine the upper limit of temperature relative to full size transition curves where elastic plastic fracture becomes invalid. This study endeavours to acquire this ratio using finite element techniques.

The development of the plastic zone in dynamic tear (DT) specimens and a non-standard three point bending fracture test specimen used to measure fracture properties was the main focus of the study. The ABAQUS finite element software was used to model the elastic-plastic behaviour of the specimens. For the DT specimen, a crack was induced by pressing the notch, followed by fatigue cracking at a limit load level of 40% of the specimen limit load, whereas, the crack shape for the non-standard specimen was a fatigue crack defined at approximately 30% of the limit load. The shapes of these cracks were adequately modelled in the finite element analysis. The specimens were made of 350WT steel and 304 stainless steel materials. The specimens were loaded until fixed amounts of permanent deformation were recorded. Results were obtained in the form of plots, showing the progression of the plastic zone around the crack tip. For each case, the results provide the following: mid point plastic deflection, stretch zone width and plastic zone radius. The finite element results obtained were compared to experimental elastic plastic testing where available, and reasonably accurate agreement was achieved.

RÉSUMÉ

L'intégrale-J est un critère de rupture élastique-plastique qui permet de mesurer la ténacité d'un spécimen qui a subi une rupture suite à une déformation générale. Il est toutefois nécessaire de comprendre le rapport de la dimension de la phase plastique (le rayon) au degré d'émoussement de la tête de fissure (la zone d'allongement) afin d'établir la limite supérieure de température, par rapport aux courbes de transition à l'échelle, à laquelle la rupture élastique-plastique n'est plus valable. La présente étude s'efforce de déterminer ce rapport à l'aide de l'analyse par éléments finis.

L'étude mettait l'accent sur la croissance de la phase plastique dans des éprouvettes ayant subi l'essai dynamique de déchirement (éprouvettes DT), ainsi que dans une éprouvette non standard ayant subi un essai de rupture avec pliage en trois points et utilisée pour mesurer les propriétés de fracture. La modélisation du comportement élastique-plastique des éprouvettes a été effectuée à l'aide du logiciel d'analyse par éléments finis ABAQUS. Dans le cas de l'éprouvette DT, une fissure a été causée par la pression exercée sur l'entaille, suivie d'une fissuration de fatigue à un niveau équivalent à 40 % de la charge limite de l'éprouvette, alors que la forme de la fissure dans l'éprouvette non standard correspondait à une fissure de fatigue équivalant à environ 30 % de la charge limite. L'analyse par éléments finis a permis de bien modéliser la forme de ces fissures. Les éprouvettes étaient composées d'acier 350WT et d'acier inoxydable 304. Elles étaient mises à l'essai jusqu'à l'obtention de valeurs constantes de déformation permanente. Les résultats obtenus montrent, sous forme graphique, la propagation de la phase plastique dans la tête de fissure. Les résultats fournissent, pour chaque cas, le fléchissement plastique au point milieu, la largeur de la zone d'allongement et le rayon de la phase plastique. Les résultats de l'analyse par éléments finis ont été comparés aux données expérimentales disponibles pour des essais de déformation élastique-plastique et la concordance était raisonnablement précise.

ACKNOWLEDGEMENTS

The authors would like to acknowledge the contributions of Dr. E.C Oguejiofor of St. Francis Xavier University and Mr. Putu Deskarta of Daltech, Dalhousie University for their assistance in the use of the ABAQUS code.

TABLE OF CONTENTS

ABSTRACT	ii
ACKNOWLEDGEMENTS	iii
TABLE OF CONTENTS	iv
LIST OF FIGURES	v
1. INTRODUCTION	1.1
1.1 Background	1.1
1.2 Objectives and Scope	1.2
2. PROBLEM DESCRIPTION	2.1
2.1 Specimen Configurations	2.1
2.2 Crack Tip Shape	2.1
2.3 Requirements	2.2
3. FINITE ELEMENT MODEL	3.1
3.1 Finite Element Approach	3.1
3.2 Finite Element Meshes	3.1
3.3 Material Models	3.1
3.3.1 350WT Steel	3.3
3.3.2 304 Stainless Steel	3.3
3.4 Boundary Conditions and Loading	3.4
4. RESULTS AND DISCUSSIONS	4.1
4.1 DT Specimen with 350 WT Steel Material	4.1
4.2 DT Specimen with 304 Stainless Steel Materials	4.3
4.3 NS Specimen with 304 Stainless Steel Material	4.4
5. SUMMARY, CONCLUSIONS AND RECOMMENDATIONS	5.1
5.1 Summary and Conclusions	5.1
5.2 Recommendations	5.1
6. REFERENCES	6.1

LIST OF FIGURES

Figure 1.1	Typical Transition Curve.....	1.3
Figure 1.2	Configuration of DT Specimen	1.3
Figure 1.3	Idealization of Plastic Zone Around Crack Tip.....	1.4
Figure 3.1	Shape of Fatigue Crack in DT Specimens.....	3.5
Figure 3.2	FE Mesh of DT Specimens	3.6
Figure 3.3	FE Mesh of Nonstandard (NS) Specimens.....	3.7
Figure 3.4	Stress-Strain Curves for 350WT Steel	3.8
Figure 3.5	Stress-Strain Curves for 304 Stainless Steel	3.9
Figure 4.1	Midpoint Displacement Responses of DT-350WT Specimen, with Flat and Rising Stress-Strain Curve Models	4.6
Figure 4.2	von Mises Stress and Equivalent Plastic Strain Development, in DT-350WT Specimen with Rising Stress-Strain Curve Model	4.7
Figure 4.3	Plastic Zone Configuration of DT-350WT Specimen Showing Area with Greater than 15% Plastic Strain at 7.87 kN (0.53 P_L)	4.12
Figure 4.4	Plastic Radius of DT-350WT Specimen	4.13
Figure 4.5	Stretch Zone Width of DT-350WT Specimen	4.13
Figure 4.6	Ratio of Plastic Radius to Stretch Zone Width of DT-350WT Specimen.....	4.13
Figure 4.7	Midpoint Displacement Response of DT-304SS Specimen, Rising Curve Model.....	4.14
Figure 4.8	von Mises Stress Development in DT-304SS Specimen with Rising Stress-Strain Curve Model	4.15
Figure 4.9	Plastic Zone Configuration of DT-304SS Specimen Showing Area With Greater Than 5% Plastic Strain at 6.88 kN (1.01 P_L)	4.18
Figure 4.10	Comparison of Plastic Zone Radius	4.18
Figure 4.11	Comparison of Stretch Zone Width.....	4.19
Figure 4.12	Comparison of Plastic Radius to Stretch Zone Width.....	4.19
Figure 4.13	Midpoint Displacement Response of NS-304SS Specimen With Rising Stress-Strain Curve	4.20
Figure 4.14	Correcting for Local Deformations in NS-304SS Specimen	4.20
Figure 4.15	Plastic Zone Configurations of NS-304SS Specimens With Rising Stress-Strain Curve Model	4.21
Figure 4.16	Plastic Zone Configuration of NS-304SS Specimen Showing Area With Greater Than 5% Plastic Strain at 4.85 kN (0.74 P_L)	4.27

1. INTRODUCTION

1.1 Background

The J-integral is one of several criteria used to determine the fracture toughness of materials. This is a criterion that is suitable for measurement of fracture in the elastic-plastic regime of the full transition curve (Figure 1.1). It permits measurements of fracture toughness of specimens that have been fractured after general yielding, and assumes that onset of fracture is due to a critical level of stress or strain being achieved at or near the crack tip [1,2]. The J-integral is measured using three-point bend specimens, such as the dynamic tear (DT) test specimens. An understanding of the ratio of the plastic zone size (radius) to the crack tip blunting (stretch zone width) is required to determine the upper limit of temperature relative to the full size transition curves where elastic-plastic fracture (J-integral) becomes invalid.

Figure 1.2 shows a typical DT specimen and Figure 1.3 shows idealizations of the plastic zone around the crack tip. As shown in Figure 1.3, the plastic zone radius is the maximum extent of the plastic zone, and the stretch zone width (SZW) is the distance from the crack tip to the interface of the plastic zone with the side of the crack. The shear lip size is given by the distance from the yield surface to the original surface on the side of the specimen. The standard validity criterion for stipulates that

$$a, b, B = 50J / \sigma_{flow} \quad (1.1)$$

This suggests that B be greater than $50J/\sigma_{flow}$. But blunting is approximately $J/(2\sigma_{flow})$. Therefore the thickness B should be greater than 100 times the critical blunting for a valid test. Thus, if the ratio of plastic zone size to blunting size is known, then the following relations will hold for a valid fracture test:

$$\begin{aligned} B &> 100SZW \\ B &> 100r_y / \beta \\ B &> 100s / \beta \text{ (or } s < B\beta / 100) \end{aligned} \quad (1.2)$$

where r_y = plastic radius, $\beta = r_y/SZW$, S is the shear tip size and the flow stress σ_{flow} is given by $\sigma_{flow} = (\sigma_y + \sigma_u)/2$, where σ_y is the yield stress and σ_u the ultimate stress. Accordingly, in the present study, the key is to identify the ratio of plastic zone size to stretch zone width. Four methods of verification are available:

- (i) Analytical (after Rice[3], who suggested the ratio was as low as 5 and as high as 600;
- (ii) Visual (after experiments on stainless steel at DREA);
- (iii) Experience in valid J testing (after DREA investigations); and
- (iv) By finite element (looking at plastic deformation of the center of the bar, stretch zone or blunting, plastic zone, and the parameter s which actually includes the shear lip and lateral contraction).

1.2 Objectives and Scope

The focus of this study is to utilize the finite element methodology to investigate the plastic zone development in three point bend fracture specimens. The aim of the study is to provide an understanding of the ratio of the plastic zone size (radius) to crack tip blunting (stretch zone width), in order to be able to predict the upper limit where elastic plastic fracture becomes invalid. Of interest is the investigation of the plastic zone development in standard dynamic tear (DT) test specimens with 350WT or 304 stainless steel materials; and a non-standard (NS) three-point bend specimen made of 304 stainless steel material.

Chapter 2 provides detailed descriptions of the specimen configurations considered in the study, and a description of the crack tip shape. The finite element methodology utilized in the investigation is presented in Chapter 3, which provides details of the finite element meshes, materials constitutive models, boundary and loading conditions, and the solution methodology. The finite element results are presented in Chapter 4, with discussions of the results. Finally, Chapter 5 provides a summary of the study and the conclusions reached.

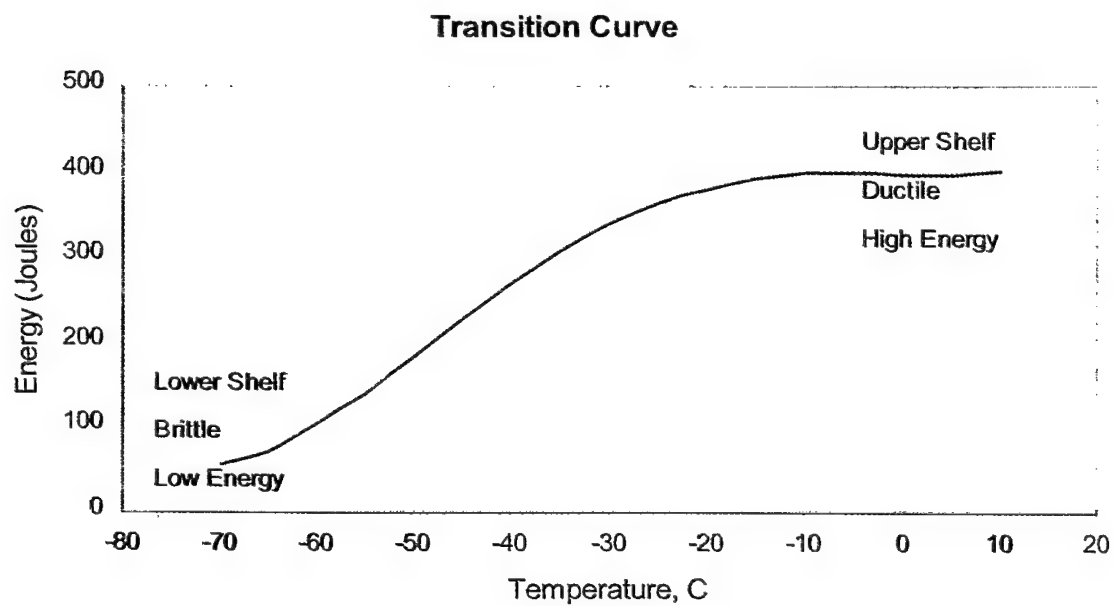


Figure 1.1: Typical Transition Curve

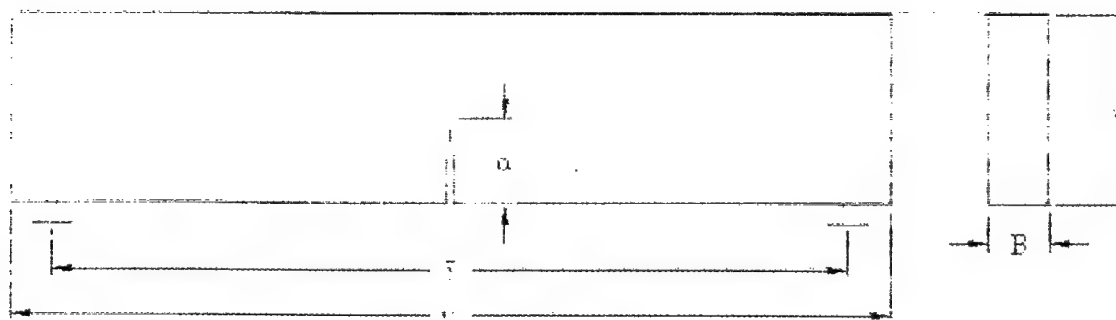


Figure 1.2: Configuration of DT Specimen

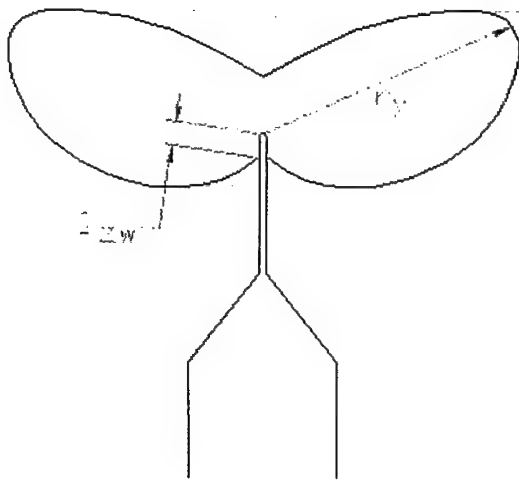


Figure 1.3(a)

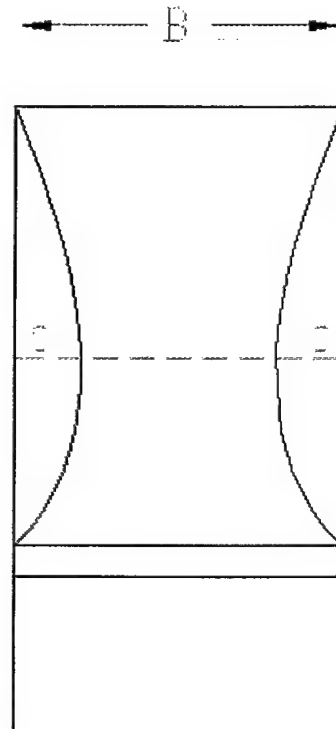


Figure 1.3(b)

Figure 1.3: Idealization of Plastic Zone Around Crack Tip

2. PROBLEM DESCRIPTION

2.1 Specimen Configurations

A schematic representation of the test specimen was presented in Figure 1.2. In the present study, three test specimens are analyzed. These include the following:

- (i) DT specimen with 350WT steel, designated as DT-350WT;
- (ii) DT specimen with 304 stainless steel, designated as DT-304SS; and
- (iii) Non-standard specimen with 304 stainless steel, designated as NS-304SS.

The DT specimens (DT-350WT and DT-304SS) had the following geometric properties:

L	=	181 mm;
S	=	164 mm;
a	=	12 mm plus .010 inches pressing followed by fatigue extension of 13 to 20 mm;
W	=	41 mm; and
B	=	8 mm.

The non-standard specimen had the following configuration:

L	=	125 mm;
S	=	100 mm;
a	=	12.5 mm fatigue crack produced by rigorous process (to be included in FE model);
W	=	25 mm; and
B	=	12.5 mm

Where

L	=	length of beam;
S	=	span of beam between supports;
W	=	width of beam;
B	=	thickness of beam; and
a	=	notch size (fatigue sharpened)

2.2 Crack Tip Shape

The crack tip shape is that of a fatigue crack initially and a blunted fatigue crack thereafter.

2.2

For the DT specimen the notch is first machined with an included angle of 60° followed by a pressing process that extends the notch 0.254 mm (0.010) with an included angle of 40° and a resulting crack tip radius of 0.254 mm (0.001). This is followed by fatigue cracking at a load level of no more than 40% of the current specimen limit load. This produces a sharp fatigue crack of definable dimensions, which we would like to use in the FE simulation. This pre-cracking extends the pressed notch by at least 1 mm.

The crack tip shape for the non-standard specimen is that of a well established fatigue crack whose maximum loading has been defined by careful laboratory fatiguing (maximum load approximately 30% of the limit load). The shape of the resulting crack tip and the configuration of the crack along its entire length were acquired by sectioning. Changes in shape of the crack tip as the FE model is run from one plastic boundary condition to another are compared to detailed laboratory metallographic measurements. Detailed descriptions of the precracking process is available in Reference [4].

2.3 Requirements

It was required to compute the progression of the plastic zone around the crack tip under quasi-static loading conditions, for the three specimens. For each case, the following response parameters were required:

- (i) Mid point plastic deflections relative to S and L mentioned above;
- (ii) Stretch zone width (i.e. distance from crack tip to interface of yield zone with side of crack); and
- (iii) Plastic zone radius (i.e. locus and maximum extent of plastic zone).

3. FINITE ELEMENT MODEL

3.1 Finite Element Approach

The prediction of the response behaviour of the DT specimen requires a tool that accounts for large geometry change and plasticity effects in the crack tip region. There are several commercial FEA tools that can be employed or adapted for calculating the stresses and strains needed. In this study the ABAQUS finite element software [5] was used to model the elastic-plastic behaviour of the DT specimen. The software has a wide range of non-linear materials models and can account for large strains and displacements. Moreover, it has been successfully used for the analysis of similar problems [6-8]. However, the HyperMesh [9] general-purpose pre- and post-processing program was used for model generation and results processing. Details of the finite element model are provided below.

3.2 Finite Element Meshes

As stated above, the HyperMesh code was used to generate the finite element models of the DT and non-standard specimens, which were then translated to ABAQUS input files. The exact shapes of the crack were obtained from DREA to enable accurate modelling of the structural configuration. Figure 3.1 shows the shape of the fatigue crack in the DT specimen. This shape had to be modelled accurately to provide meaningful results. Detailed 2-D finite element models of the specimen were developed. In order to reduce the problem size only one-half of the structure was modelled. The finite element models of the DT and non-standard (NS) specimens are as shown in Figures 3.2 and 3.3, respectively. Plane strain elements were used to model the structure. These elements allow for the treatment of large displacements, finite strains and plasticity, which are expected to occur in the specimen.

3.3 Material Models

An incremental rate independent plasticity theory available in the ABAQUS finite element program [5] was used for the material constitutive model. This standard model for

plasticity is summarized here for completeness. The total multi-axial strain state ϵ_{ij} , expressed in terms of elastic and plastic components, was

$$\epsilon_{ij} = \epsilon_{ij}^e + \epsilon_{ij}^p \quad (3.1)$$

The total logarithmic uniaxial strain, ϵ , consistent with the integration of the rate of deformation tensor for a multiaxial strain state, is decomposed as

$$\epsilon = \epsilon^e + \epsilon^p \quad (3.2)$$

The yield function f is related to uniaxial tension by

$$f(\tau_{ij}) = \tau(\epsilon^p) \quad (3.3)$$

where τ_{ij} and τ are the multiaxial Kirchhoff and uniaxial stress states, respectively. The associated flow rule, dissipation equivalence condition and a consistency condition govern plastic strain increments.

The specific form of f is the von Mises yield function

$$f(\tau_{ij}) = \left(\frac{3}{2} (S_{ij} S_{ij}) \right)^{1/2}, \quad (3.3)$$

where S_{ij} is the deviatoric component of stress.

The Kirchhoff stress and logarithmic strain measures are employed because of advantages gained in computational implementation. The Kirchhoff stress tensor, τ_{ij} , is approximately equal to the more physically motivated Cauchy stress tensor, σ_{ij} , for deformations involving only small changes in volume [7,8]. This condition is implicit in the current elastic-plastic analysis. The uniaxial Cauchy stress-logarithmic strain constitutive response of the material are formally

input, in multilinear form, as Cauchy stress and logarithmic plastic strain pairs for the ABAQUS program. The constitutive parameters for the 350WT and 304SS materials are described below.

3.3.1 350WT Steel

The material for the first DT specimen was 350WT steel. The engineering stress-strain curve for this material was obtained from DREA. This curve terminated at a strain of 25%. However, from experimental investigations by DREA [10], strains as high as 250% were observed around the crack tip of the specimen. A method for defining the stress-strain behaviour beyond 25% strain was therefore required. Two possible stress-strain curves, as illustrated in Figure 3.4, were considered. In the first model (Figure 3.4a), the stress was assumed to be constant at the maximum stress level from 25% to 250% strain. This case is referred to as the flat curve model. In the second constitutive model (Figure 3.4 (b)), the stress was assumed to rise from the maximum uniaxial test stress of about 600 MPa to 1100 MPa from 25% to 250% strain. The maximum stress value was determined from experimental observation and intuition [10]. This second case is referred to as the rising curve model.

3.3.2 304 Stainless Steel

The second DT specimen and the non-standard specimens were made of 304 stainless steel material. The stress strain curve for the material was obtained from the literature [11]. This curve terminated at a strain of about 80%. However, from experimental investigations by DREA [5], strains as high as 1000% were observed around the crack tip of the specimen. In this case only the rising curve model was used beyond the 80% strain level. The possible stress-strain curve is illustrated in Figure 3.5. In this constitutive model the stress was assumed to rise from the maximum uni-axial test stress of about 600 MPa to 1000 MPa from 80% to 1000% strain. The maximum stress value was determined from experimental observation and intuition [10].

3.4

3.4 Boundary Conditions and Loading

The following boundary conditions were applied:

At the support: $v = 0$

Along the center line: $u = 0$;

Where, u, v are the displacements components in the longitudinal and transverse directions. The load was applied as a concentrated load at the top middle point of the beam.

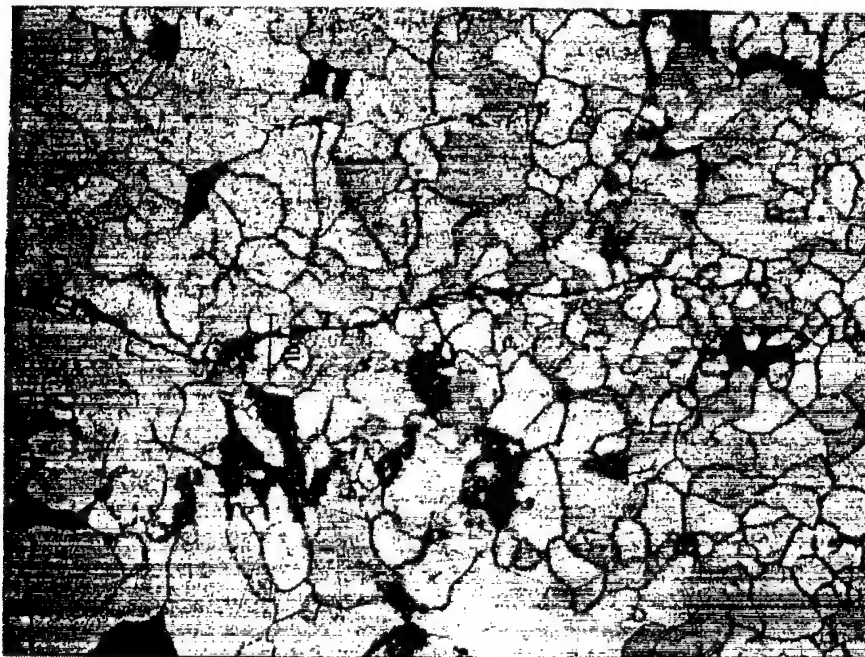


Figure 3.1: Shape of Fatigue Crack in DT Specimens

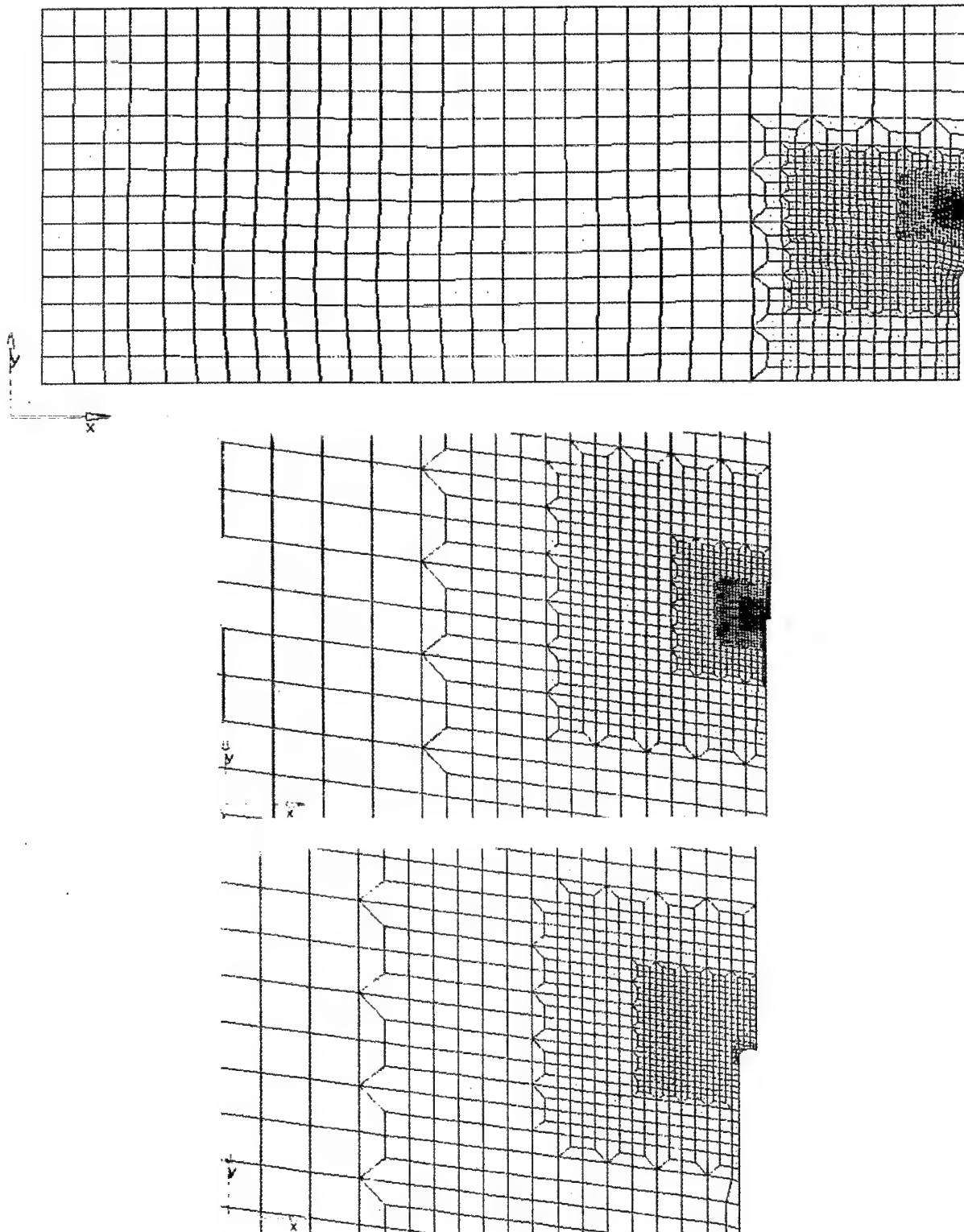


Figure 3.2: FE Mesh of DT Specimens

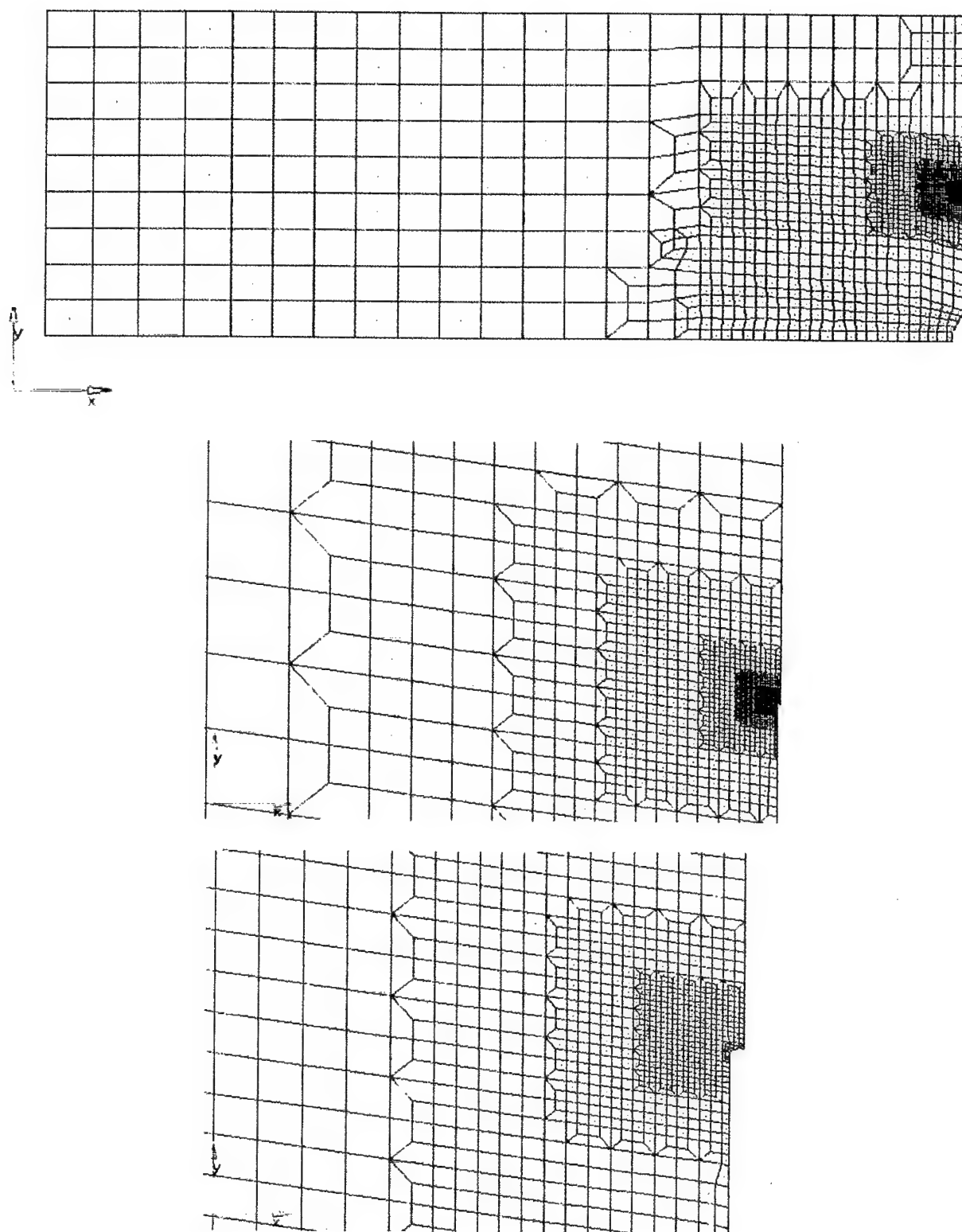
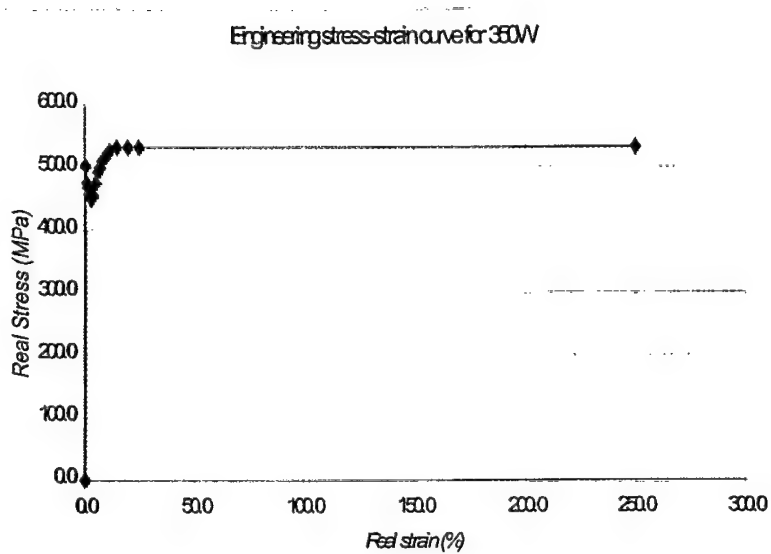
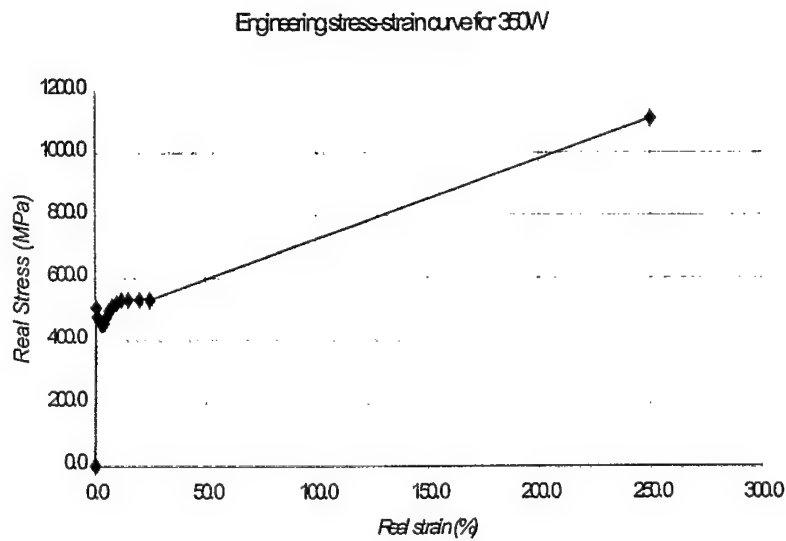


Figure 3.3: FE Mesh of Nonstandard (NS) Specimens



(a)



(b)

Figure 3.4: Stress-Strain Curves for 350WT Steel

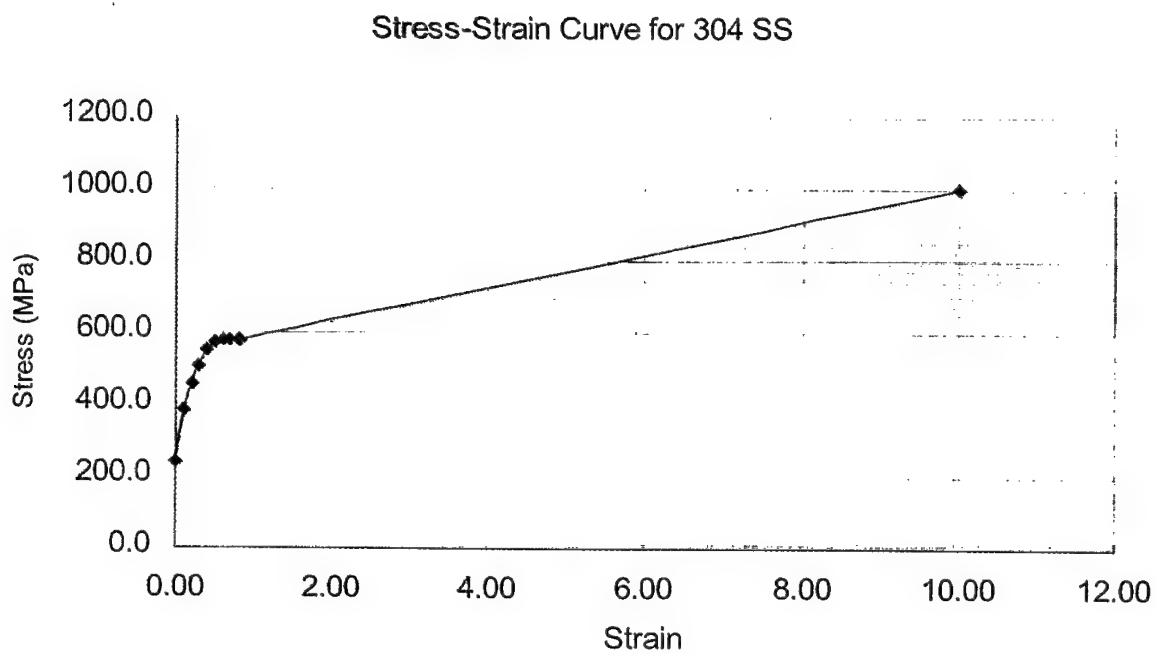


Figure 3.5: Stress-Strain Curves for 304 Stainless Steel

4. RESULTS AND DISCUSSIONS

This chapter discusses the results of the study. The finite element results obtained for the three specimen configurations are discussed in Sections 4.1 to 4.3, respectively. For each specimen, results of the midpoint displacement, plastic zone development and stretch zone width are provided.

4.1 DT Specimen with 350 WT Steel Material

Midpoint Displacements

The predicted load-displacement response of the midpoint of the beam is shown in Figure 4.1. In the figure, DL refers to the displacement of the top midpoint with respect to the top left end point, and DS refers to the bottom midpoint with respect to the support point. The results obtained from using the flat and rising stress-strain curves are all presented in the figure. It is seen that the use of a flat or rising stress-strain curve does not have any significant effect on the midpoint displacement responses. The applied load has been non-dimensionilized with respect to the limit load P_L , which is given by

$$P_L = \frac{4}{3} \left(\frac{Bb^2\sigma_y}{S} \right) \quad (4.1)$$

where B is the thickness, b is the untracked ligament ($b=W-a$), σ_y is the yield strength and S is the span between the supports. The displacement contour at the last load step for the rising curve mode is presented in Figure A1 of Appendix A.

Plastic Zone Development

The shape of the plastic zone was similar for both the flat and rising stress-strain models. However, the stress and strain levels beyond the 25% strain level were quite different for the two cases because of the different load paths. Figure 4.2 shows the development of the von Mises stresses and equivalent plastic strains in the DT-350WT material with the rising curve model, at

different load levels. For the sake of completeness, the corresponding results from the flat stress-strain curve model are presented in Figure A2 of Appendix A. For the von Mises stress plots, all regions with stresses above the yield stress of 450 MPa are shown in red, and the area that has not yielded is shown in blue. For the equivalent plastic strain plots, all other areas are shown in blue. Also, the same view is used for all the figures so a direct comparison of the shape and size of the plastic zone can be made. It is seen that the shapes and size, of the plastic zones using the von Mises stress or equivalent plastic strain are very similar. Also, as expected, the plastic zone size increased with load. In addition, the plastic zone tends to rise upwards from the tip of the crack, which is similar to the experimentally observed behaviour [2].

Figure 4.3 shows the plastic zone that has strained over 15% (when necking starts) of two load levels. In comparison with the plastic zones at the corresponding load levels in Figure 4.3, it is seen that necking occurs in only a small area around the crack tip.

Plastic Zone Radius (r_y) Stretch Zone Width (SZW) and Ratio r_y/SZW

The plastic zone radius, r_y , and the stretch zone width (SZW) at various load levels were measured from the plastic zone configurations. The plastic zone was given by the distance from the crack tip to the farthest point of the plastic zone. The stretch zone width (SZW) was given by the distance from the crack tip to the interface of the plastic zone with the side of the crack (see Figure 1.3). Figures 4.4 and 4.5, respectively show the variation of the plastic radius and SZW with load, for the flat and rising stress-strain curve models of the DT-350WT specimen. The figures show that the plastic zone radii and stretch zone widths obtained from the two models are almost identical as for the shapes of the plastic zones, as discussed above. The ratios of the plastic zone radius to stretch zone width (r_y/SZW) were also computed and presented in Figure 4.6. Again, the responses from the two constitutive models are very similar, and the ratios vary from 50 to 90. Due to the fact that the configurations of the plastic zone predicted by the flat and rising curve constitutive models were similar, only the rising curve (strain hardening) model was used for the remaining specimens, as this provided more realistic strain levels.

4.2 DT Specimen with 304 Stainless Steel Materials

Midpoint-Displacement

The predicted load-displacement response of the midpoint of the beam is shown in Figure 4.7. The displacements of the DT-304SS specimen are smaller than those of the DT-350WT specimen. For instance, at $1.1P_L$, the midpoint displacement with respect to the end point, DL, is approximately equal to 0.3mm compared to 0.63mm for the DT-350WT specimen (see Figure 4.1), since the applied load for the DT-304SS specimen (7.49 kN) was less than the load applied to the DT-350WT specimen (16 kN). The displacement contours at the last load increment are presented in Figure A3 of Appendix A.

Plastic Zone Development

Figure 4.8 shows the development of the von Mises stresses and equivalent plastic strains in the DT-304SS specimen. In the von Mises stress plots, all regions with stress above the yield stress of 240 MPa are shown in red and the area that has not yielded is shown in blue. In the equivalent plastic strain plots, all areas with plastic strains greater than 0.01% are shown in red and all other areas are shown in blue. As before, the same view is used for the plots to facilitate direct comparison. The plastic zone configurations at various load levels follow the same pattern as described for the DT-350WT specimens. The area around the crack tip that was strained by more than 15% was insignificant. So in Figure 4.9 only the area around the cracktip that is strained by more than 5% is shown. It is seen that this area is very small compared to the overall plastic zone size.

Plastic Zone Radius (r_y), Stretch Zone Width (SZW) and Ratio r_y/SZW

The plastic zone radius and SZW at various loads were measured as described in Section 4.1. Figure 4.10 shows the variation of plastic radius with load. For comparison, the plastic zone radii of the DT-350WT specimen are also shown. As shown, the plastic radii for the DT-304SS specimen follow the same trend as for the DT-350WT specimen, and the plastic radii for the two specimen are very close, with those of the DT-304SS specimen being slightly larger. Figure 4.11 show the SZW variation with load. Again, the trends of the results for the DT-304SS and DT-

350WT specimens are similar. However, the values of the SZW for the DT-304SS specimen are generally smaller than those of the DT-350WT specimen. The variation of the ratio of the plastic radius to the stretch zone width is shown in Figure 4.12, where a plot of the ratio for the DT-350WT specimen is also shown. Both ratios increase slightly with load, however, the range of the r_p/SZW for the DT-304SS specimen is 140-150 compared to 50-90 for the DT-350WT specimen, this is expected, since the 304SS material was more ductile than the 350WT steel.

4.3 NS Specimen with 304 Stainless Steel Material

Midpoint Displacement

The predicted load-displacement response of the midpoint of the beam is presented in Figure 4.13. As before, DL refers to the displacement of the midpoint with respect to the end point and DS the displacement with respect to the support. Due to the fact that the load was applied as a point load at the midpoint, significant local deformation of the midpoint was observed. To reduce the local deformation effects it would have been necessary to distribute the load over a few elements near the middle of the beam. Because of the computational effort required to do another run, an extrapolation method was devised to reduce the local effects as illustrated in Figure 4.14. With this approach, the computed midpoint displacement of the last load step (1.044PL) was 0.18 mm compared to 0.23 mm obtained experimentally [4]. The displacement contours at last load increment are presented in Figure A4 of Appendix A.

Plastic Zone Development

The predicted von Mises stresses and equivalent plastic strains at various load levels for the NS-304SS specimen are shown in Figure 4.15. The plastic zones are defined by the regions with stresses over 240 MPa or over 0.01% plastic strain. It is observed that the plastic zones predicted by using the stress or strain criterion are very similar. The same view is used for all the plots to facilitate direct comparison. Figure 4.16 shows the region around the crack with plastic strains greater than 5%. Again, these areas are quite small compared to the corresponding overall plastic zone sizes.

Plastic Zone Radius (r_p), Stretch Zone Width (SZW) and Ratio r_p /SZW

The variations of plastic zone radius and stretch zone width (SZW) with load, for the NS-304SS specimen are presented in Figures 4.10 and 4.11, respectively. For comparison, the corresponding results for the DT-350WT and DT-304SS specimens are also shown in the figures. It is observed that the plastic radius and SZW for the NS-304SS specimen are generally smaller than those of the DT-350WT and DT-304SS specimens. The variation of the ratio of plastic radius to stretch zone width is shown in Figure 4.12 along with the corresponding results for all the other specimens. The r_p /SZW ratio for the NS-304SS specimen fall generally between those of the DT-350WT and DT-304SS specimens.

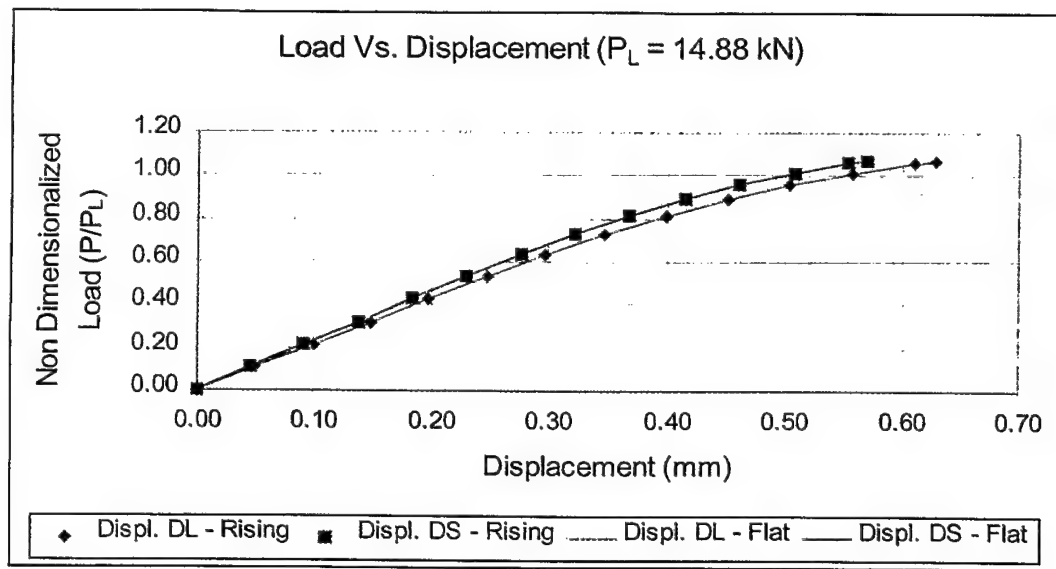
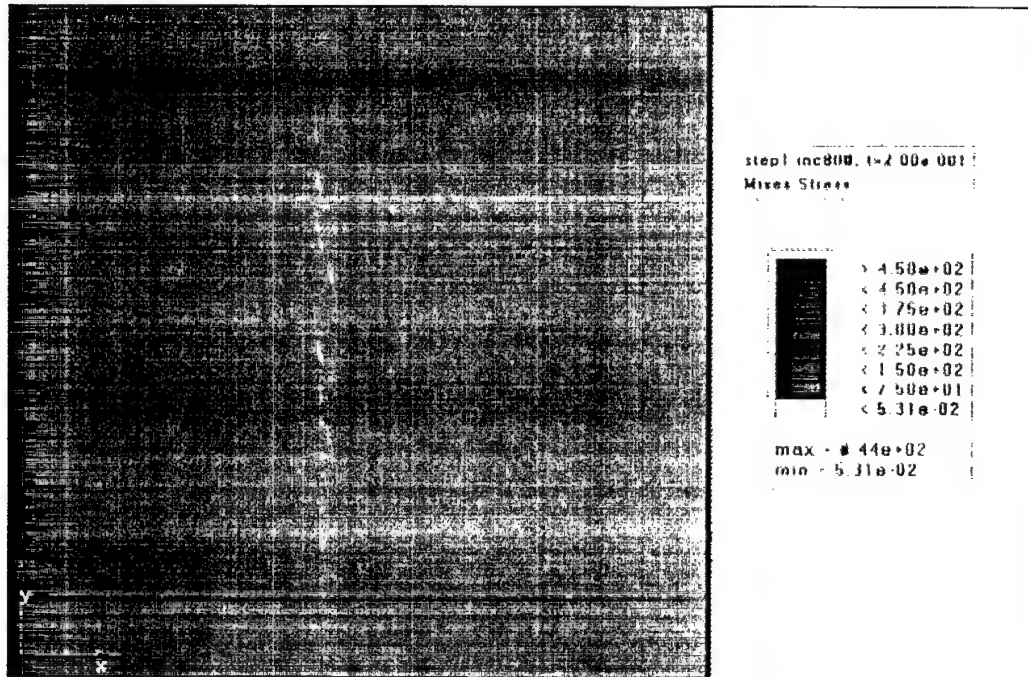
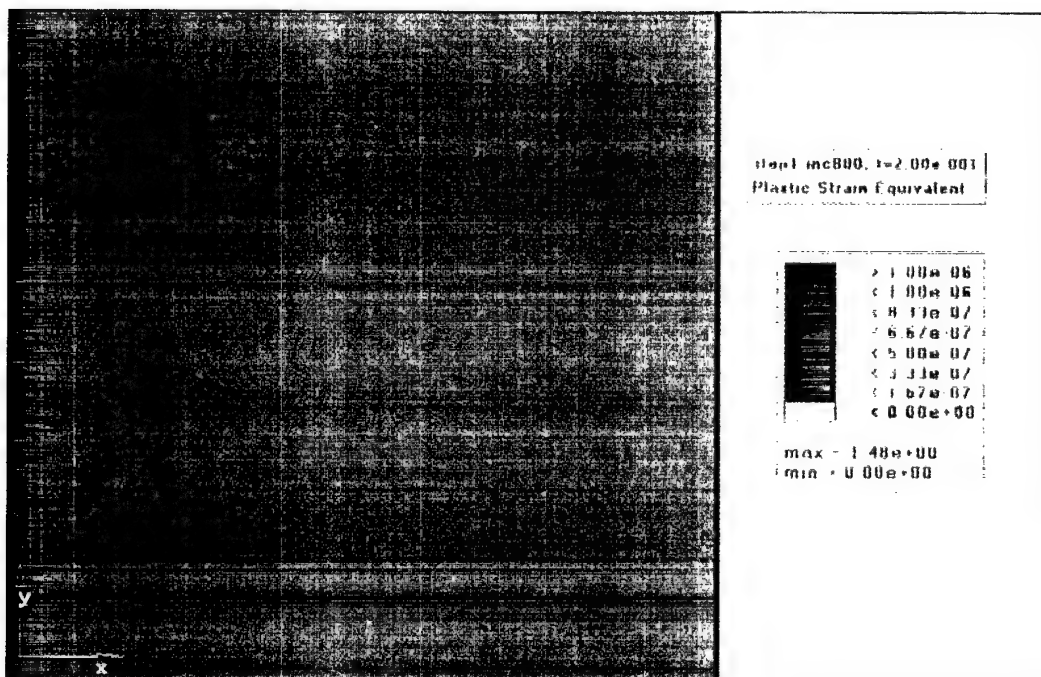


Figure 4.1: Midpoint Displacement Responses of DT-350WT Specimen, with Flat and Rising Stress-Strain Curve Models



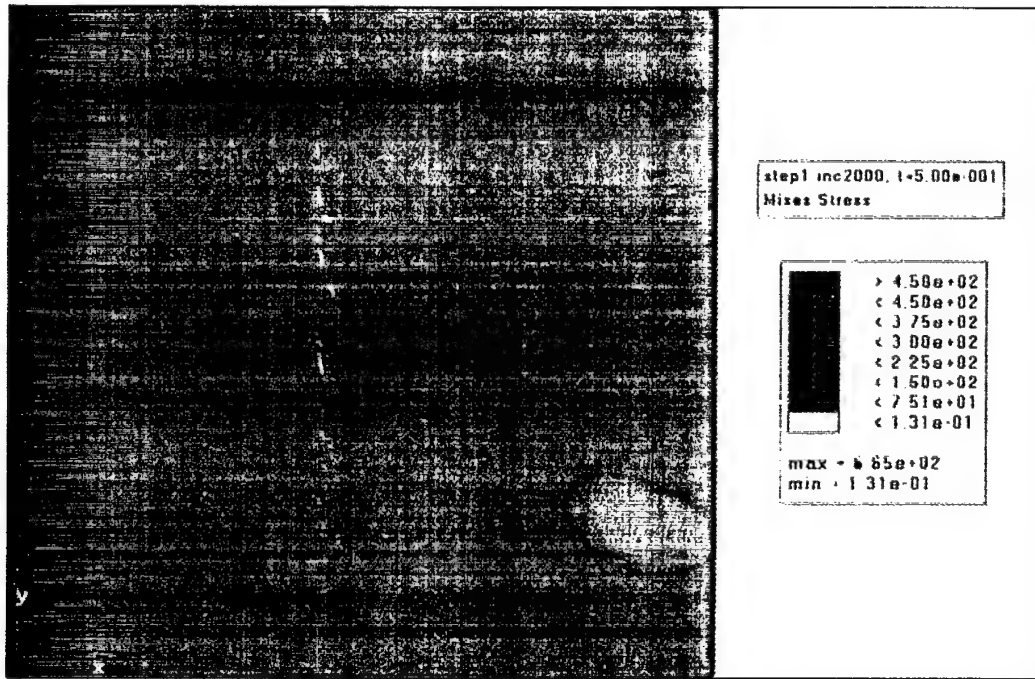
(a)



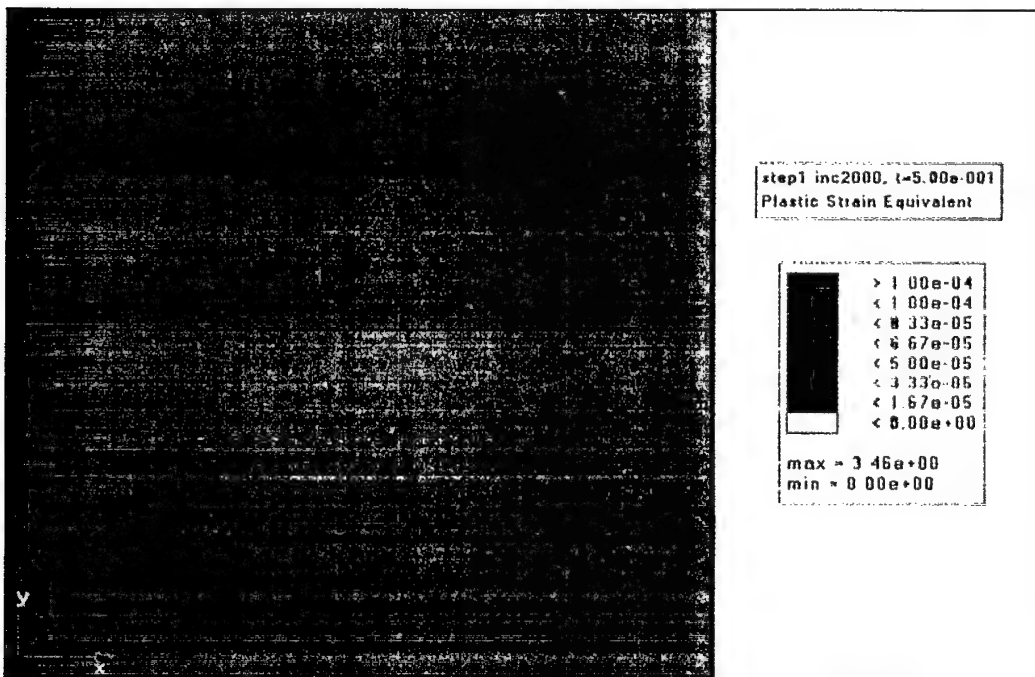
(b)

Figure 4.2: von Mises Stress and Equivalent Plastic Strain Development, in DT-350WT Specimen with Rising Stress-Strain Curve Model

(a) von Mises Stress and (b) Plastic Strain at 3.19 kN (0.21 P_L)



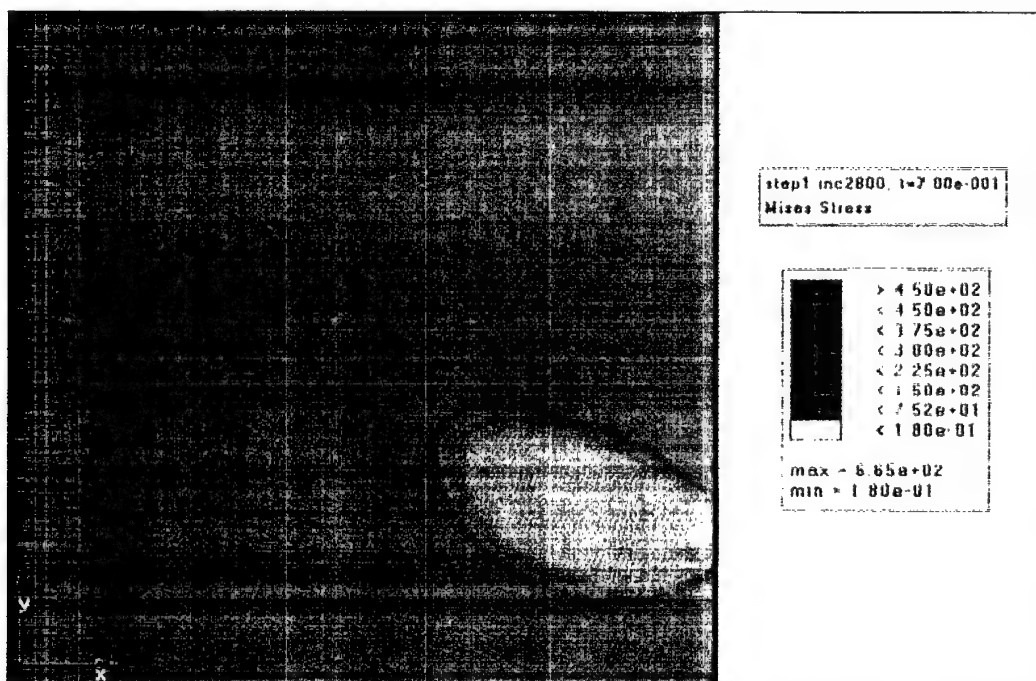
(c)



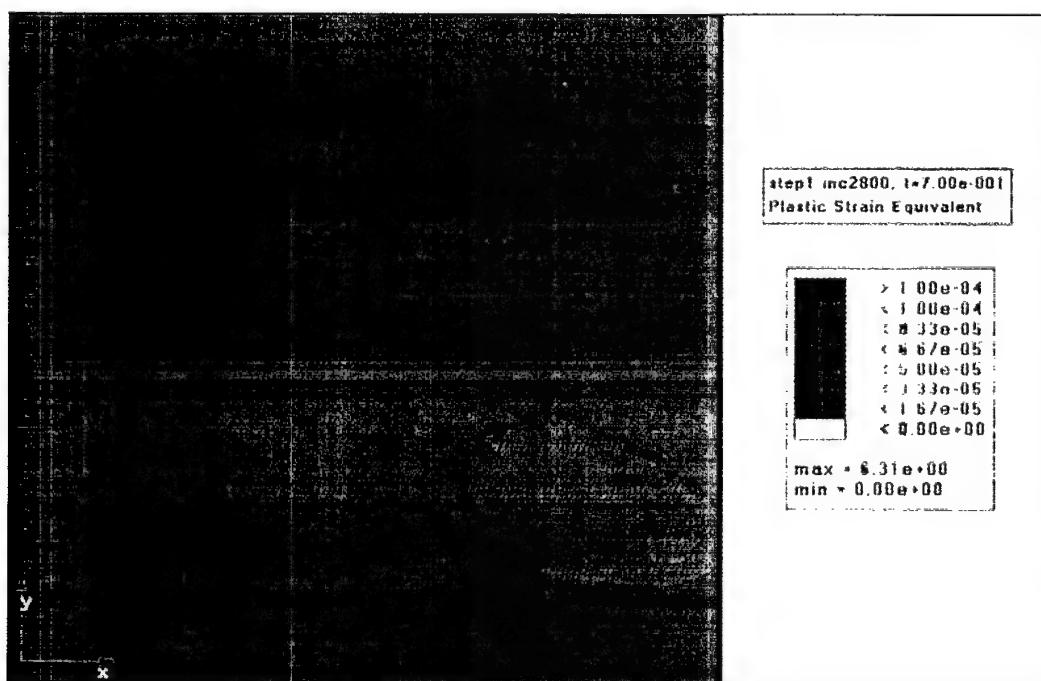
(d)

Figure 4.2 Continued: von Mises Stress and Equivalent Plastic Strain Development, in DT-350WT Specimen with Rising Stress-Strain Curve Model

(c) von Mises Stress and (d) Plastic Strain at 7.87 kN (0.53 P_L)



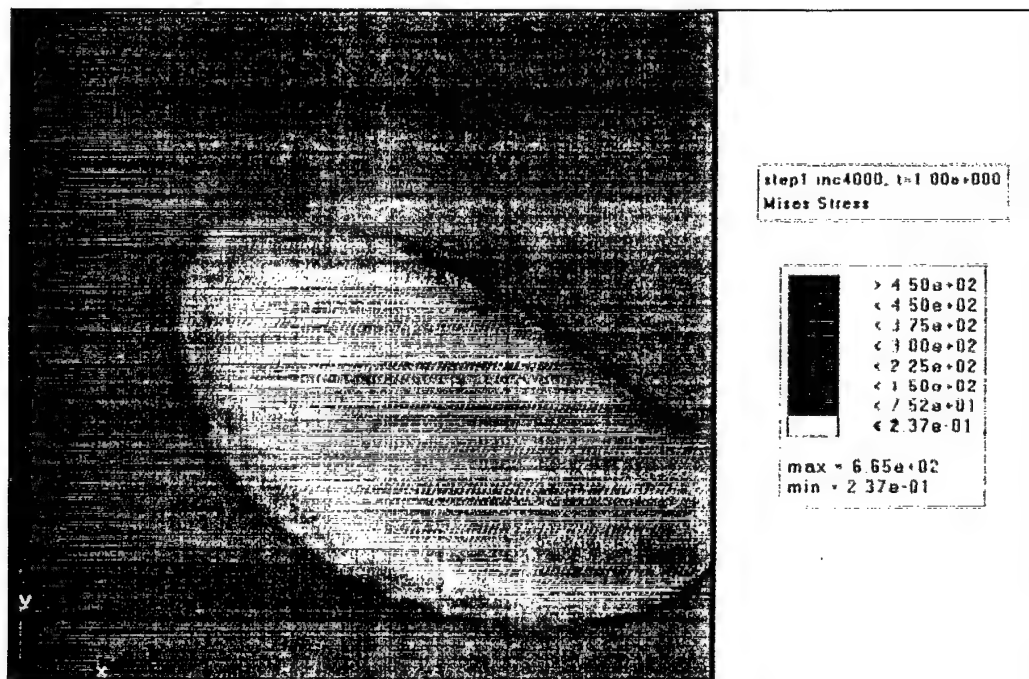
(e)



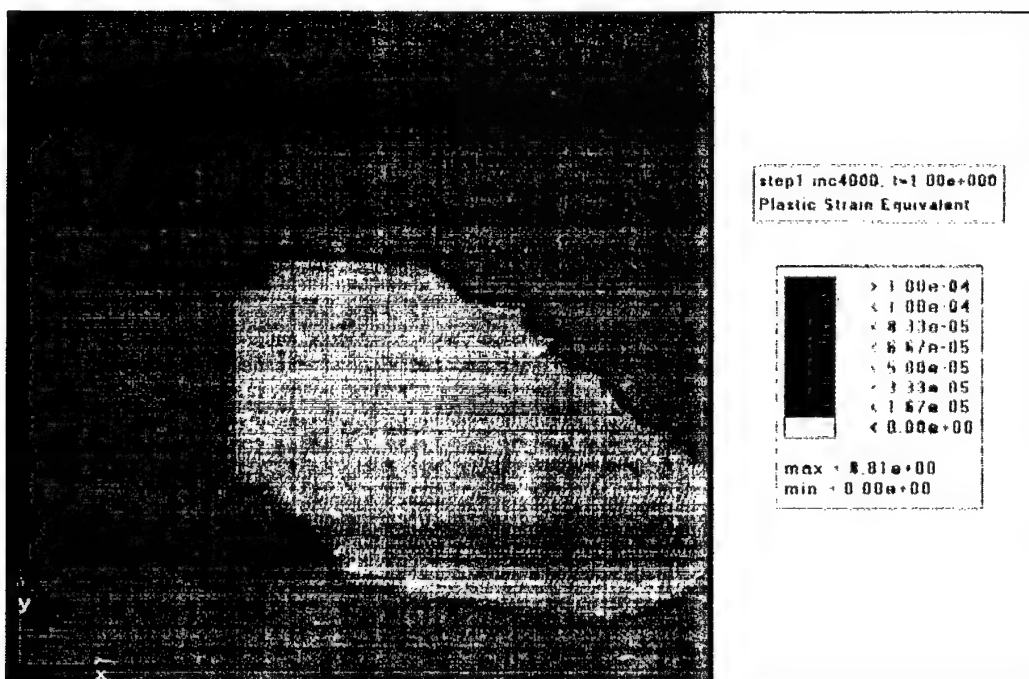
(f)

Figure 4.2 Continued: von Mises Stress and Equivalent Plastic Strain Development, in DT-350WT Specimen with Rising Stress-Strain Curve Model

(e) von Mises Stress and (f) Plastic Strain at 10.81 kN (0.73 P_L)



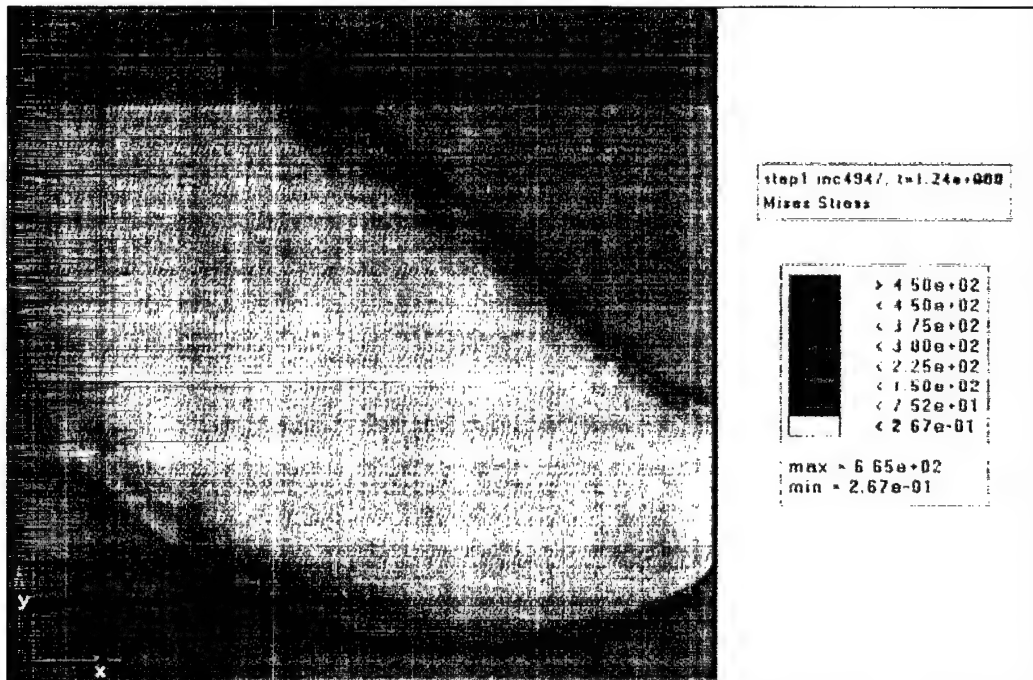
(g)



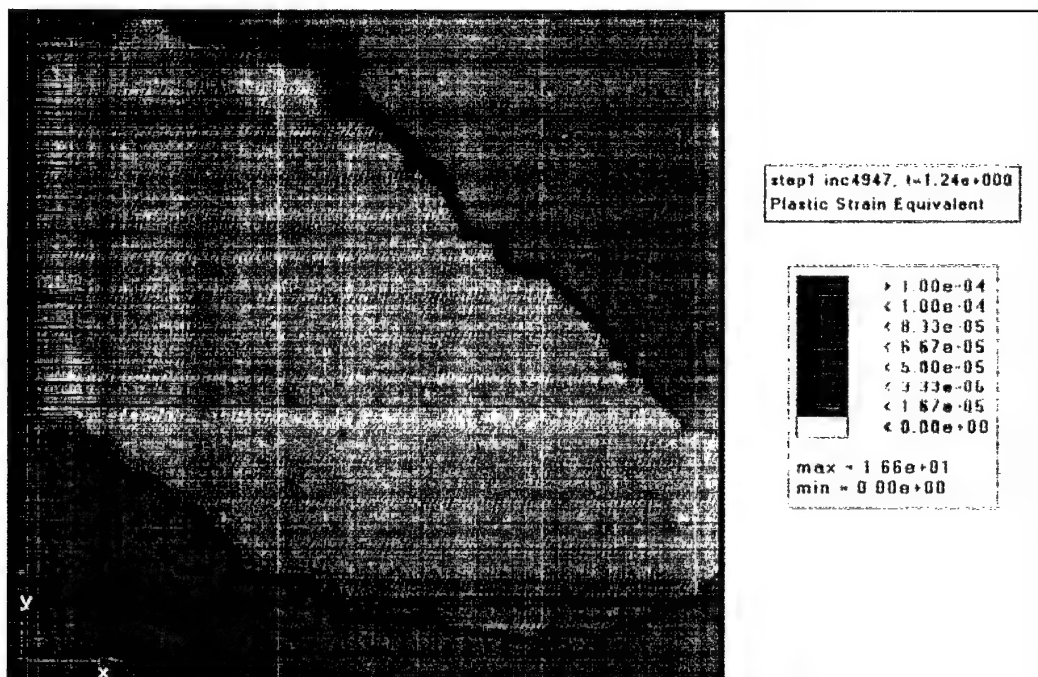
(h)

Figure 4.2 Continued: von Mises Stress and Equivalent Plastic Strain Development, in DT-350WT Specimen with Rising Stress-Strain Curve Model

(g) von Mises Stress and (h) Plastic Strain at 14.24 kN (0.96 P_y)



(i)



(j)

Figure 4.2 Continued: von Mises Stress and Equivalent Plastic Strain Development, in DT-350WT Specimen with Rising Stress-Strain Curve Model

(i) von Mises Stress and (j) Plastic Strain at 16.00 kN (1.08 P_d)

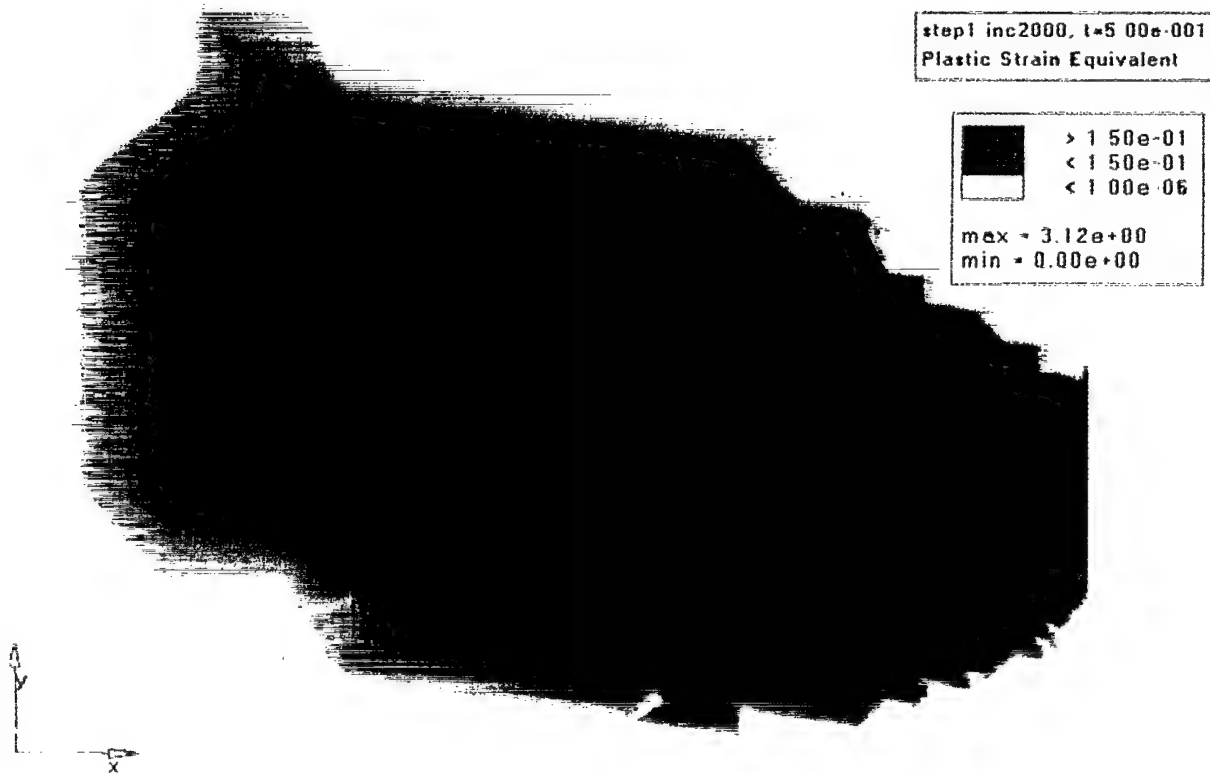


Figure 4.3: Plastic Zone Configuration of DT-350WT Specimen Showing Area with Greater than 15% Plastic Strain at 7.87 kN (0.53 P_L)

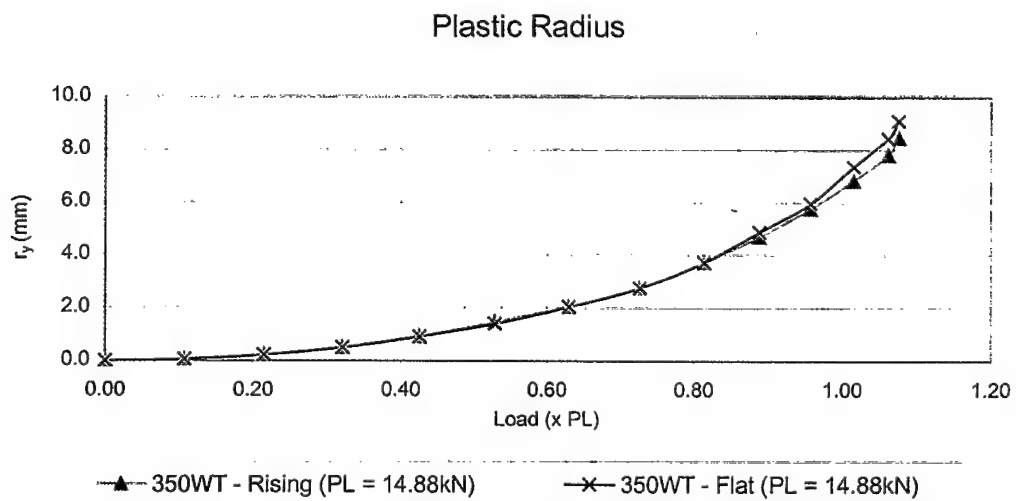


Figure 4.4: Plastic Radius of DT-350WT Specimen

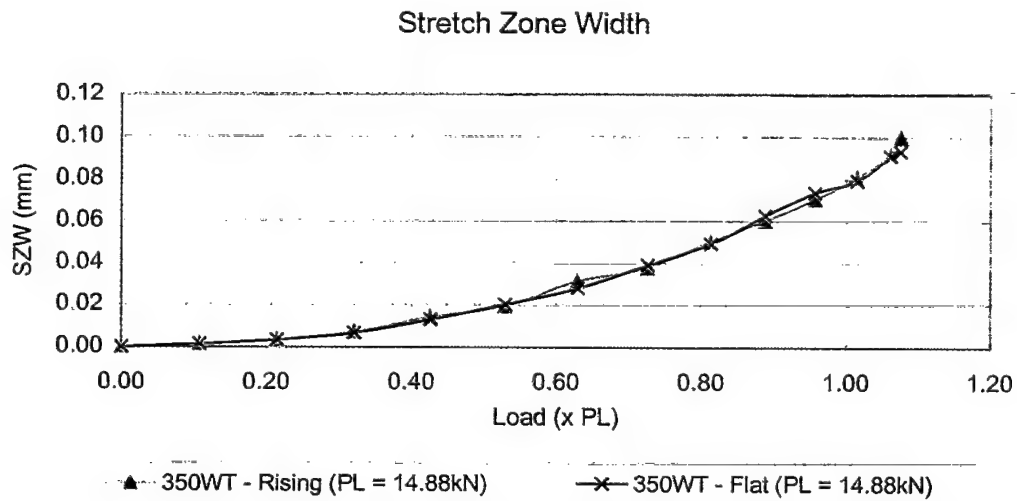


Figure 4.5: Stretch Zone Width of DT-350WT Specimen

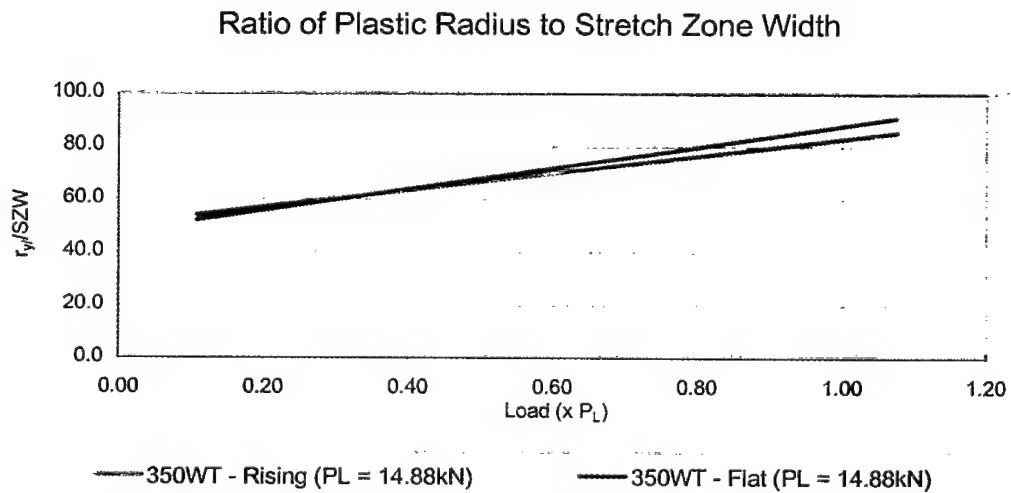


Figure 4.6: Ratio of Plastic Radius to Stretch Zone Width of DT-350WT Specimen

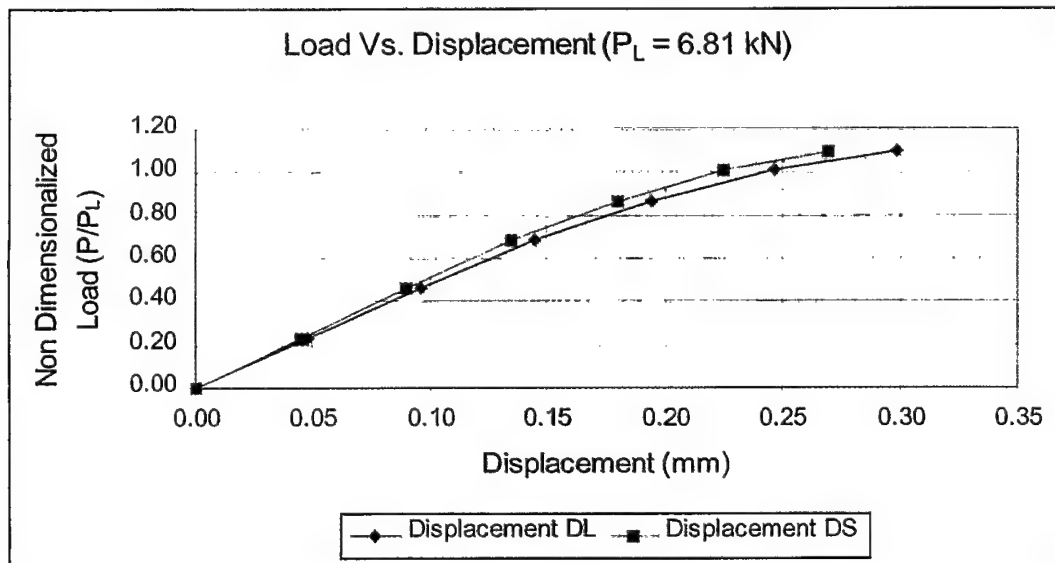
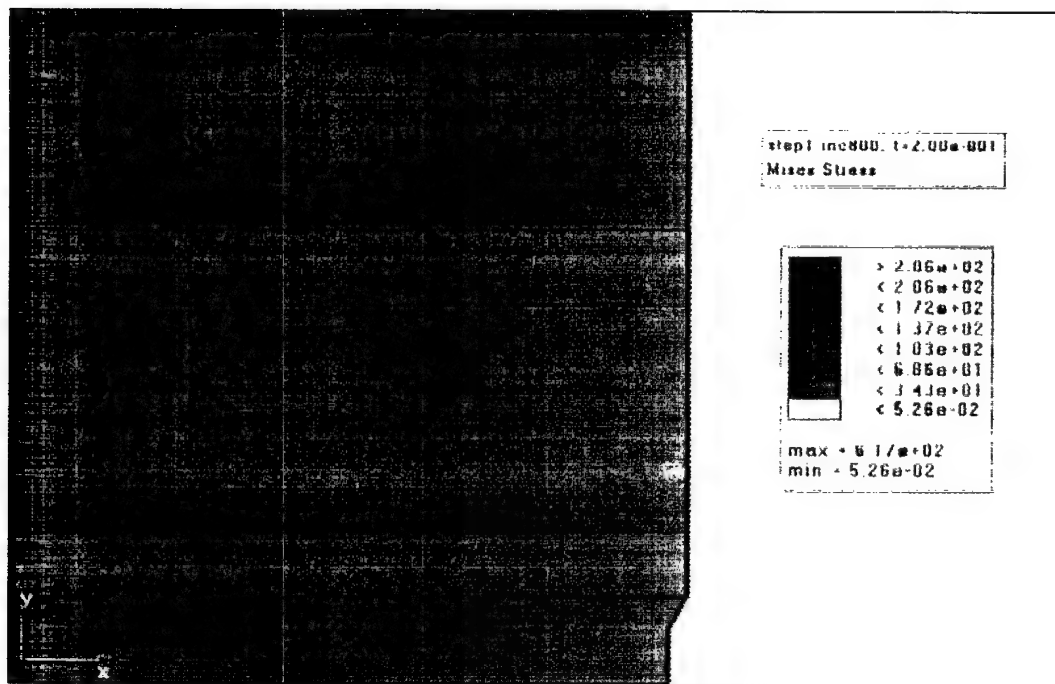
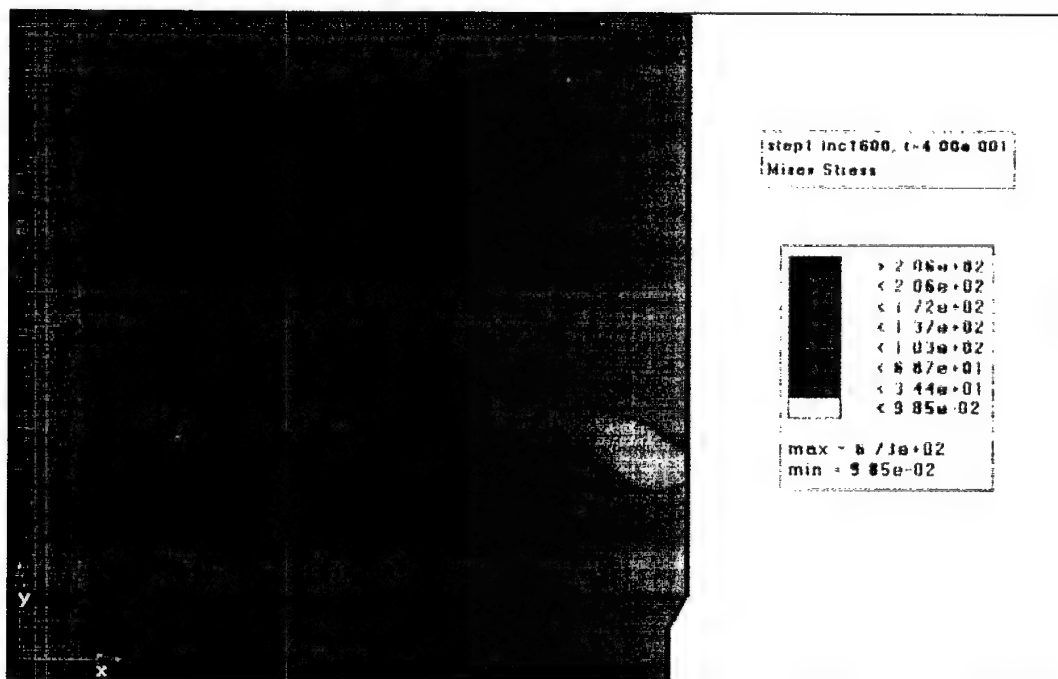


Figure 4.7: Midpoint Displacement Response of DT-304SS Specimen, Rising Curve Model



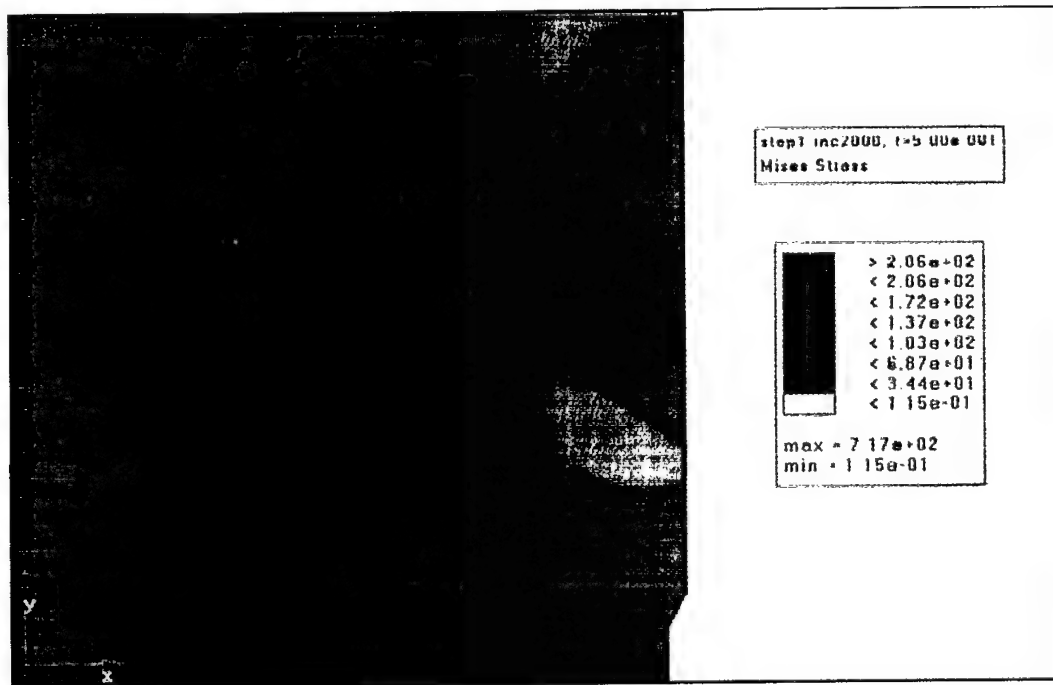
(a)



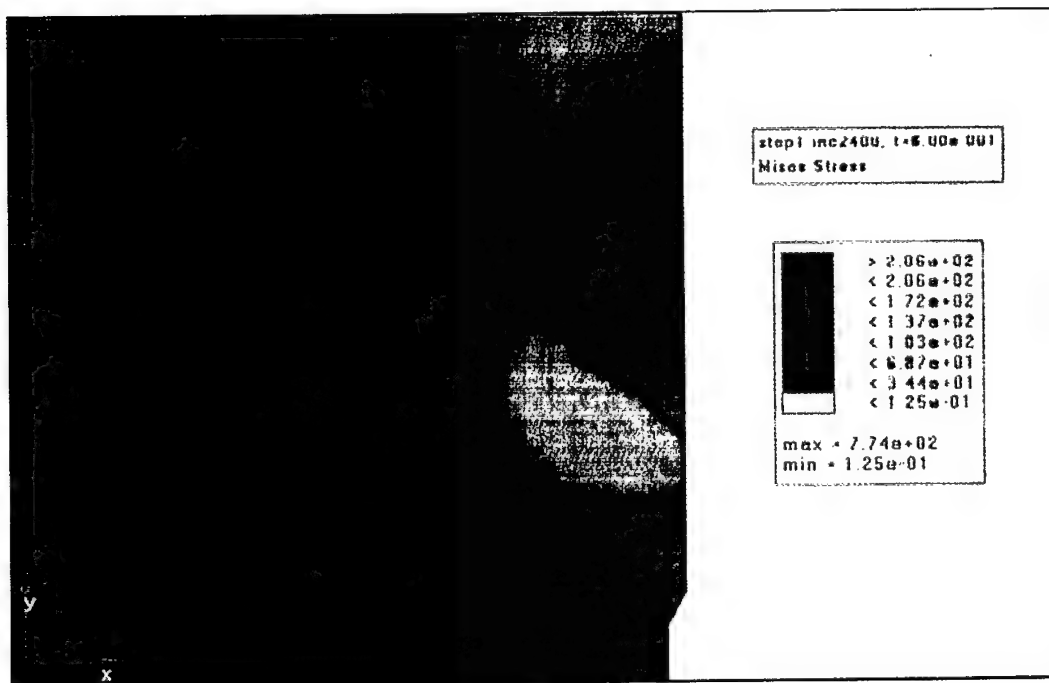
(b)

Figure 4.8: von Mises Stress Development in DT-304SS Specimen with Rising Stress-Strain Curve Model

(a) at 3.16 kN (0.46 P_L) and (b) at 5.92 kN (0.87 P_L)



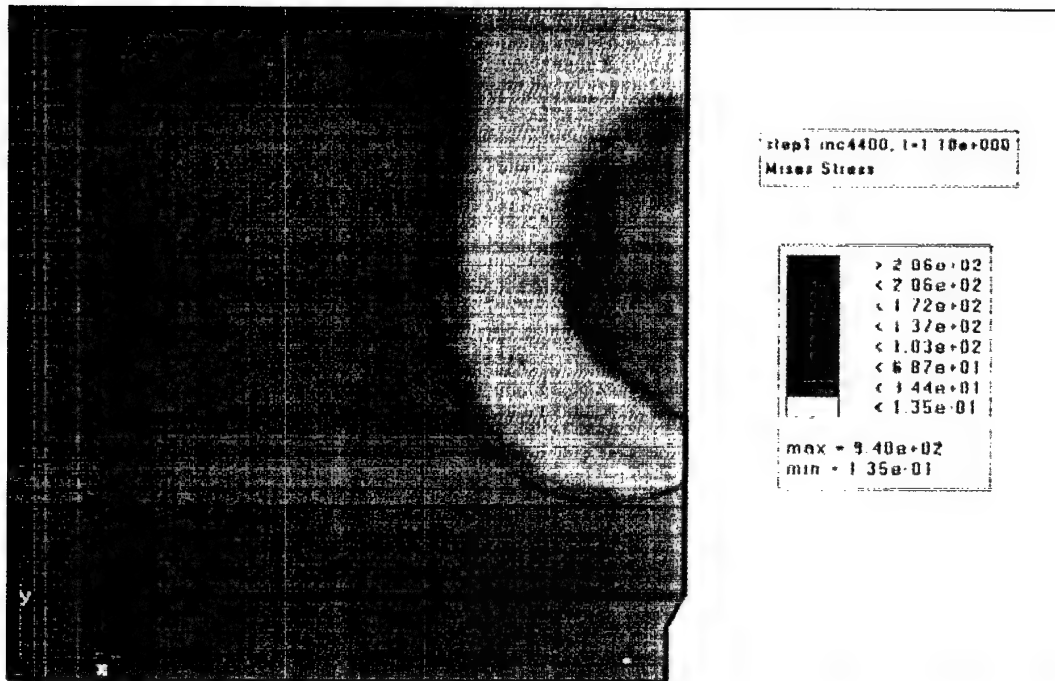
(c)



(d)

Figure 4.8 Continued: von Mises Stress Development in DT-304SS Specimen with Rising Stress-Strain Curve Model

(c) at 6.88 kN ($1.01 P_L$) and (d) at 7.48 kN ($1.10 P_L$)



(e)

Figure 4.8 Continued: von Mises Stress Development in DT-304SS Specimen with Rising Stress-Strain Curve Model

(e) at 8.10 kN (1.19 P_L)

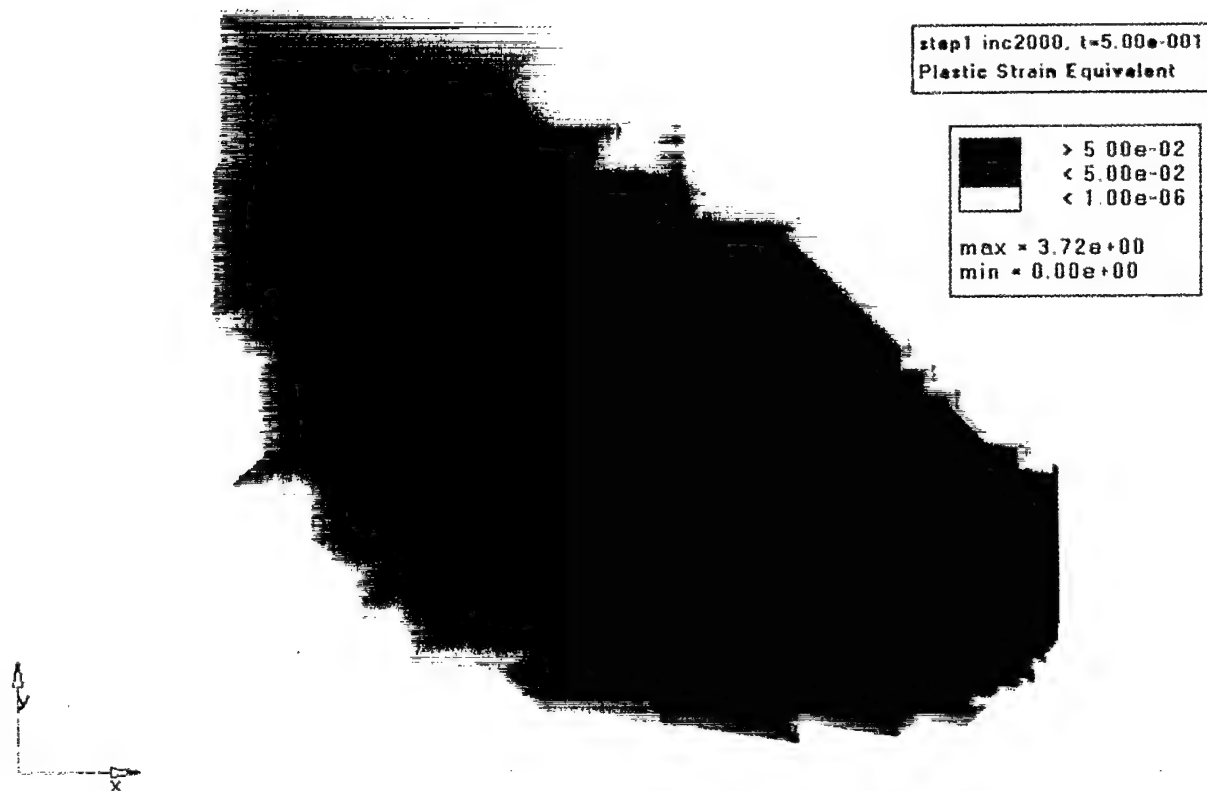


Figure 4.9: Plastic Zone Configuration of DT-304SS Specimen Showing Area With Greater Than 5% Plastic Strain at 6.88 kN ($1.01 P_L$)

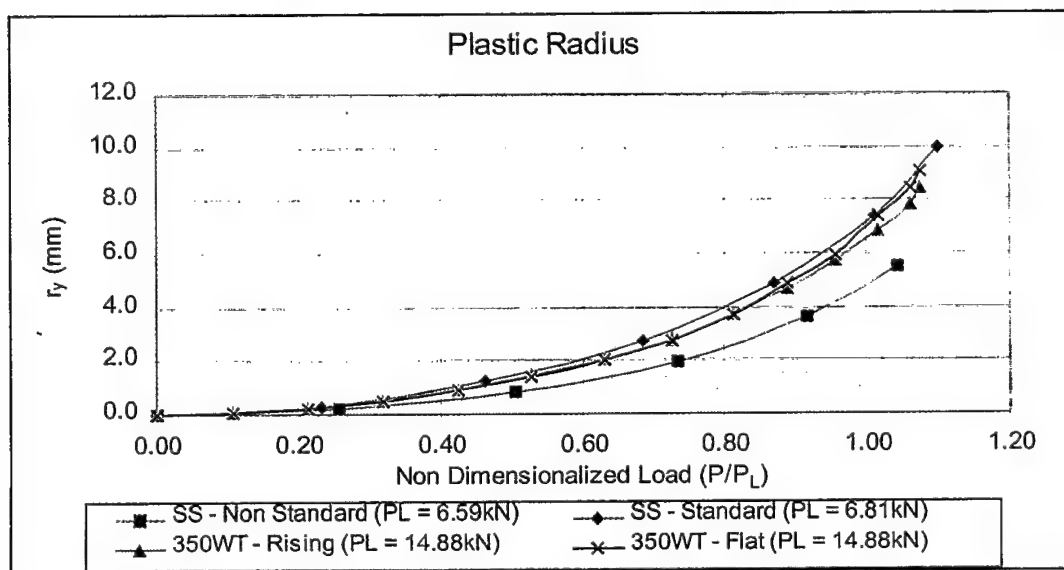


Figure 4.10: Comparison of Plastic Zone Radius

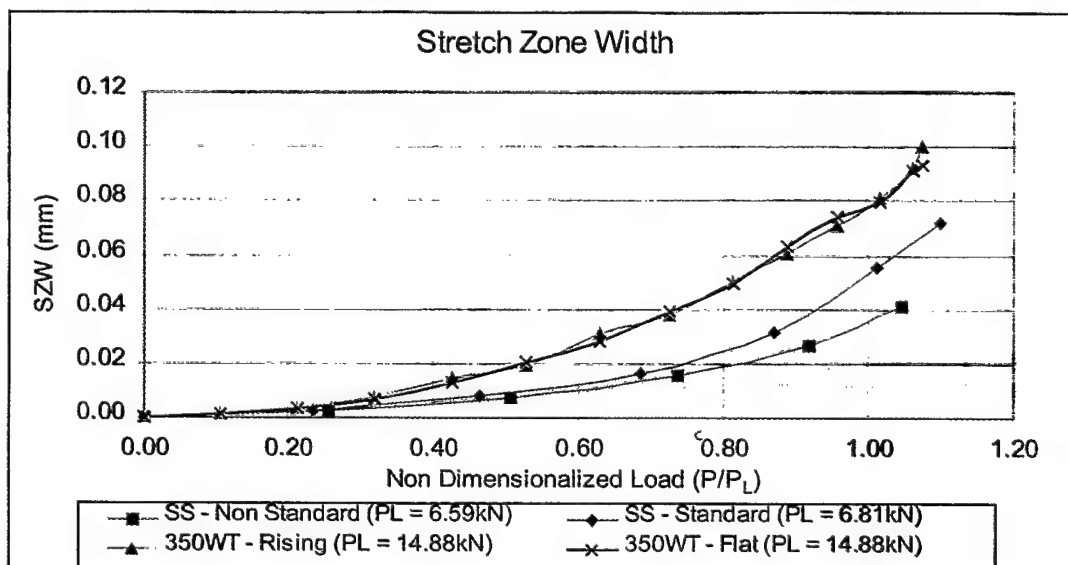


Figure 4.11: Comparison of Stretch Zone Width

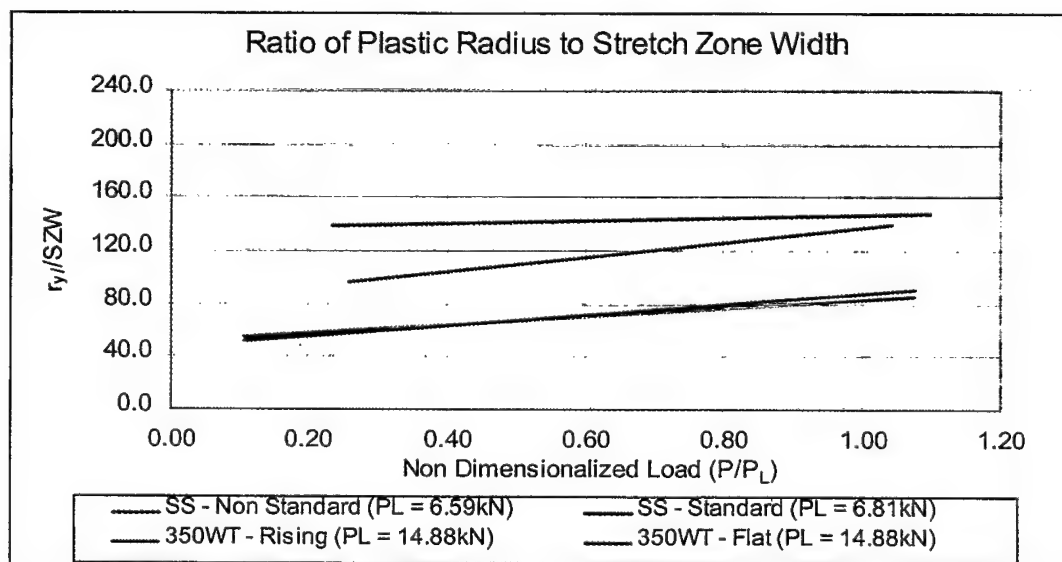


Figure 4.12: Comparison of Plastic Radius to Stretch Zone Width

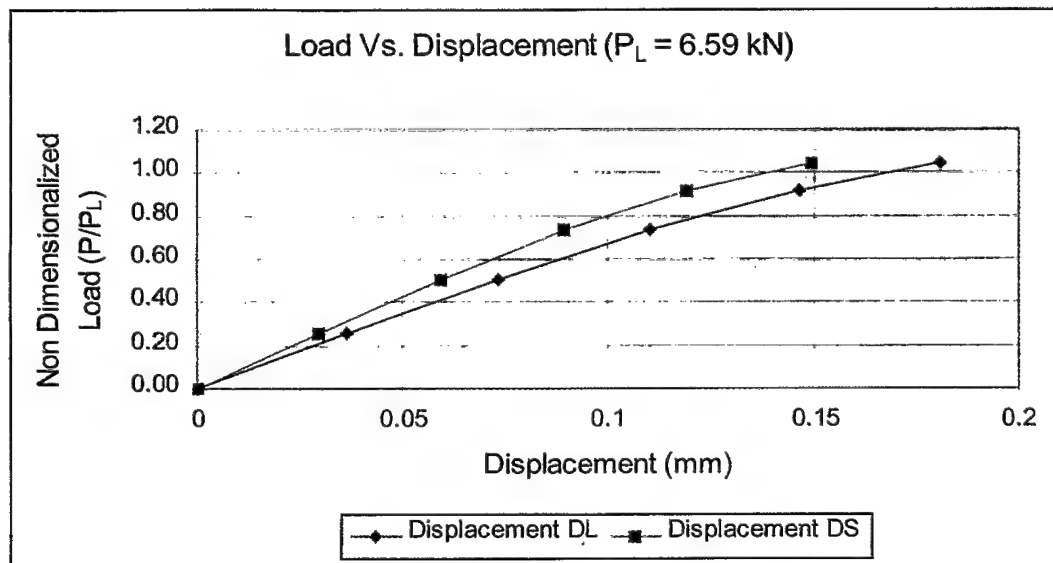


Figure 4.13: Midpoint Displacement Response of NS-304SS Specimen With Rising Stress-Strain Curve

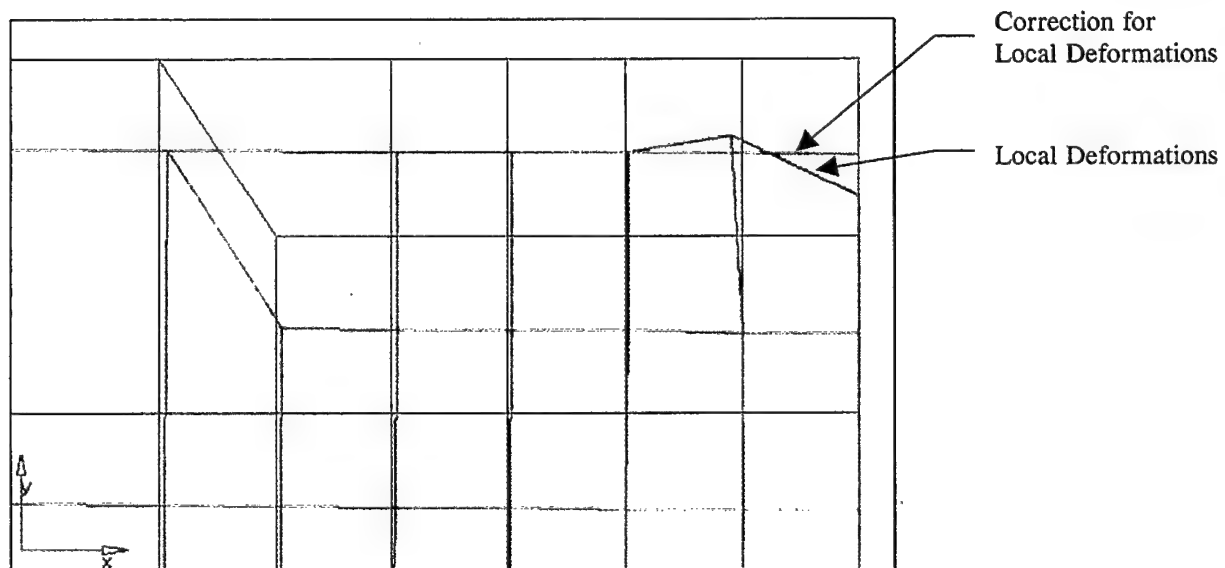
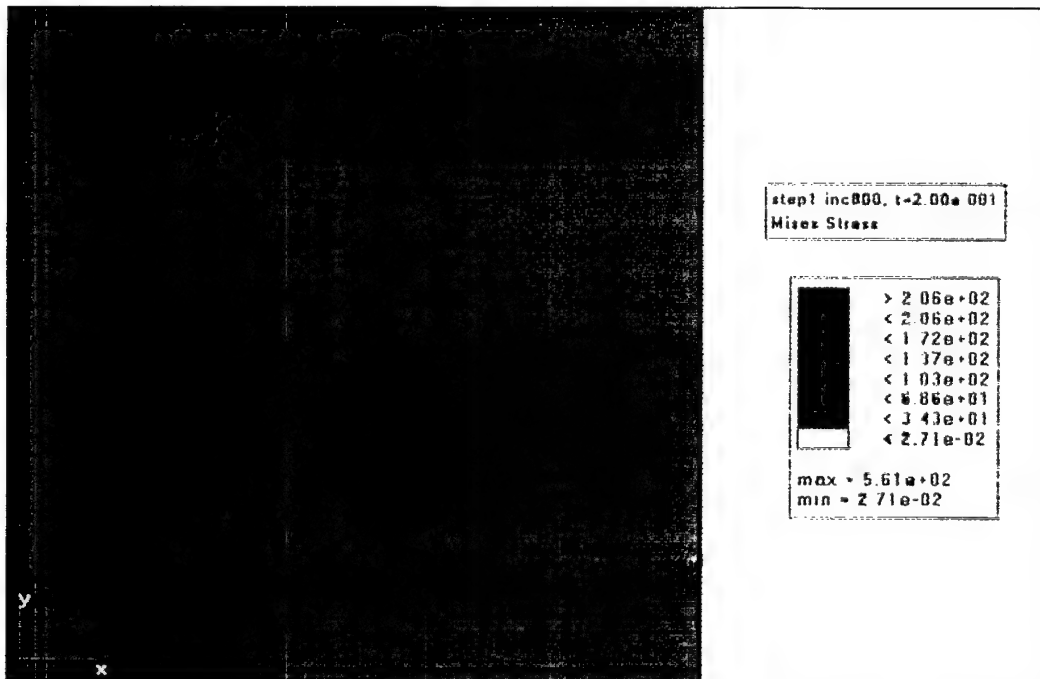
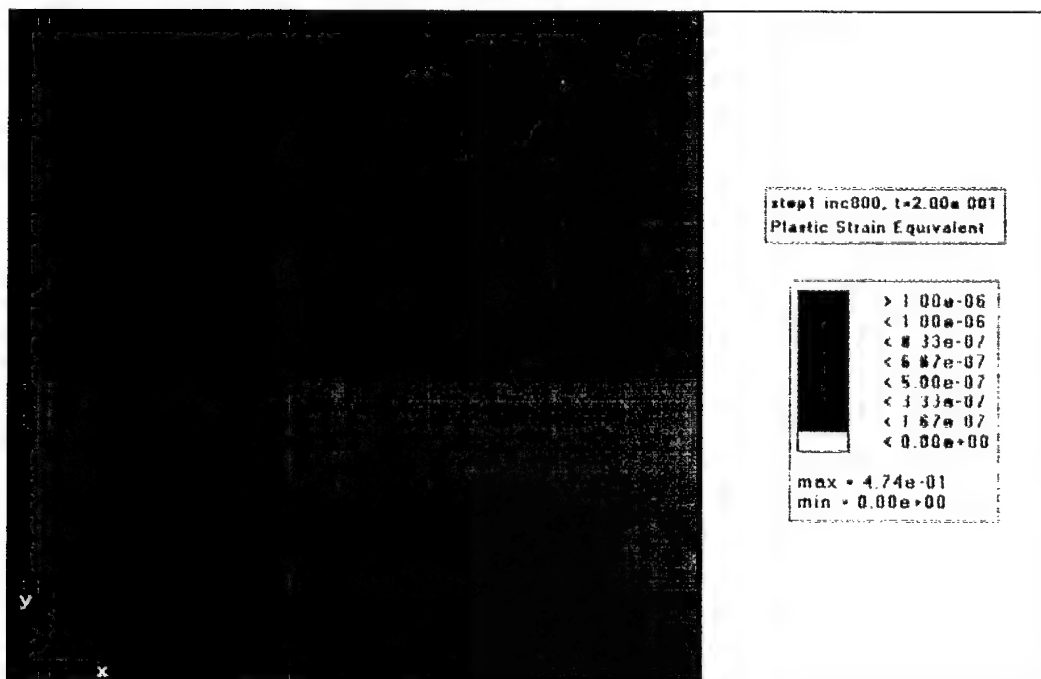


Figure 4.14: Correcting for Local Deformations in NS-304SS Specimen



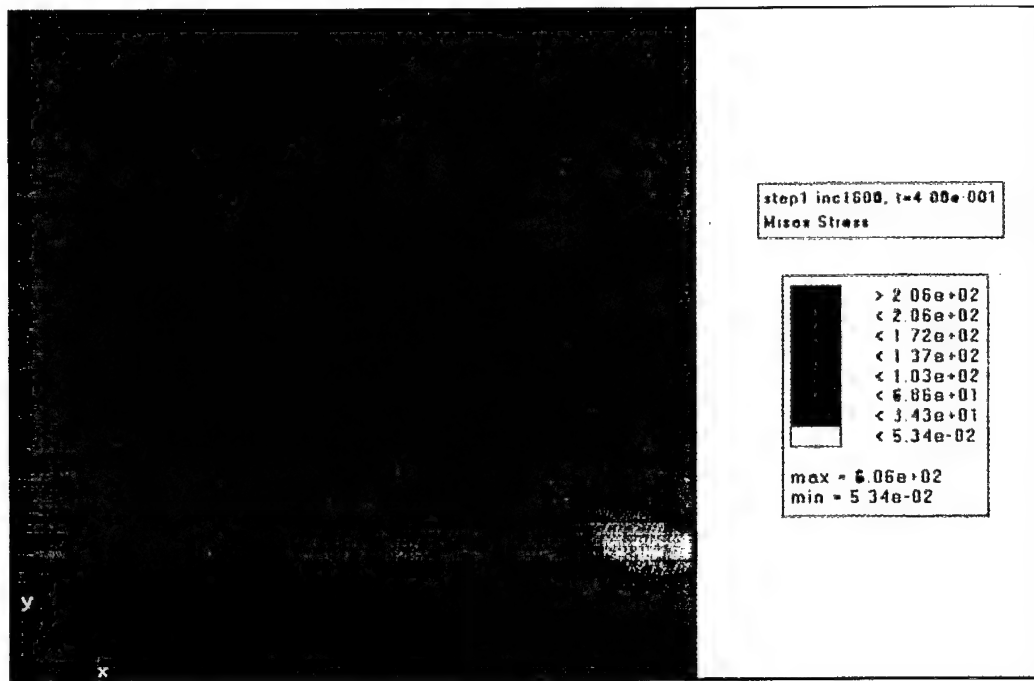
(a)



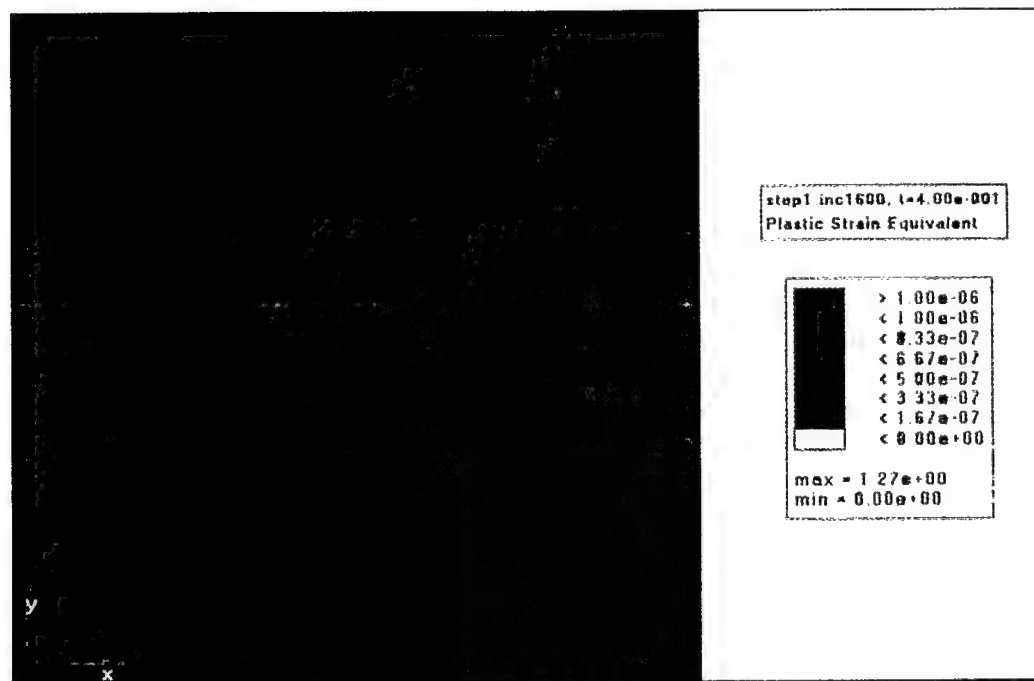
(b)

Figure 4.15: Plastic Zone Configurations of NS-304SS Specimens With Rising Stress-Strain Curve Model

(a) von Mises Stress and (b) Plastic Strain at 1.69 kN (0.26 P_L)



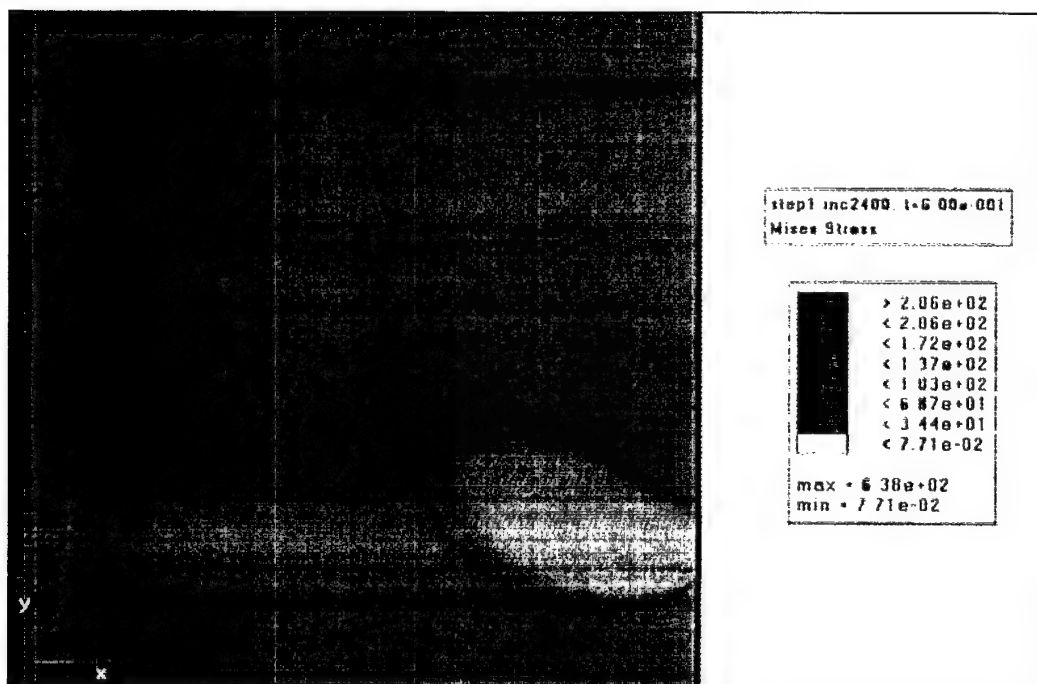
(c)



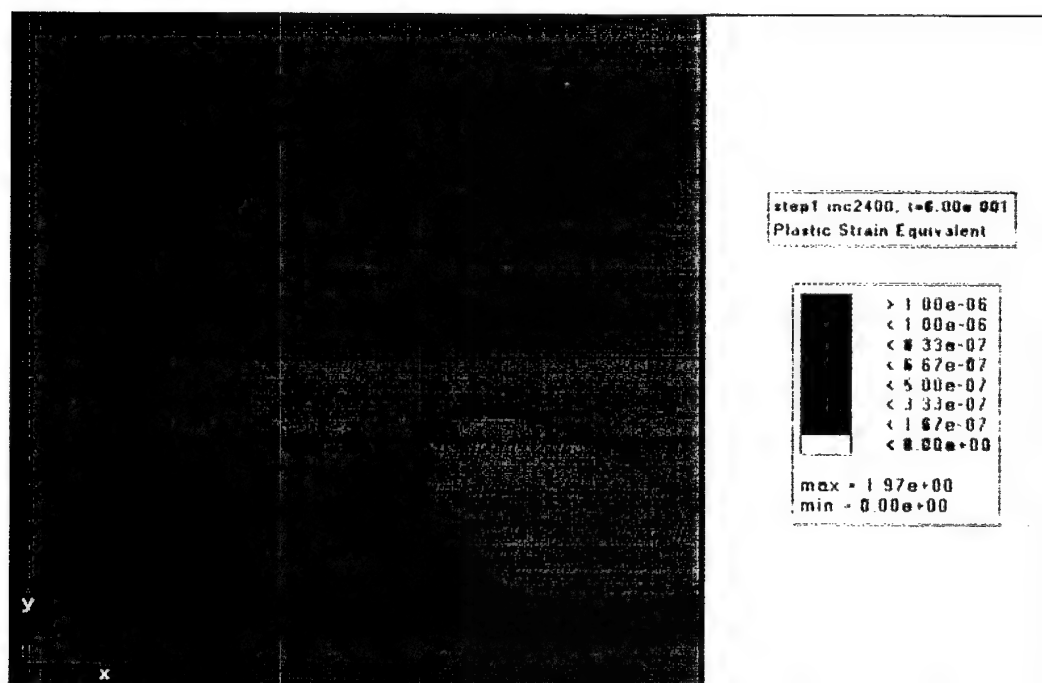
(d)

Figure 4.15 Continued: Plastic Zone Configurations of NS-304SS Specimens With Rising Stress-Strain Curve Model

(c) von Mises Stress and (d) Plastic Strain at 3.34 kN (0.51 P_L)



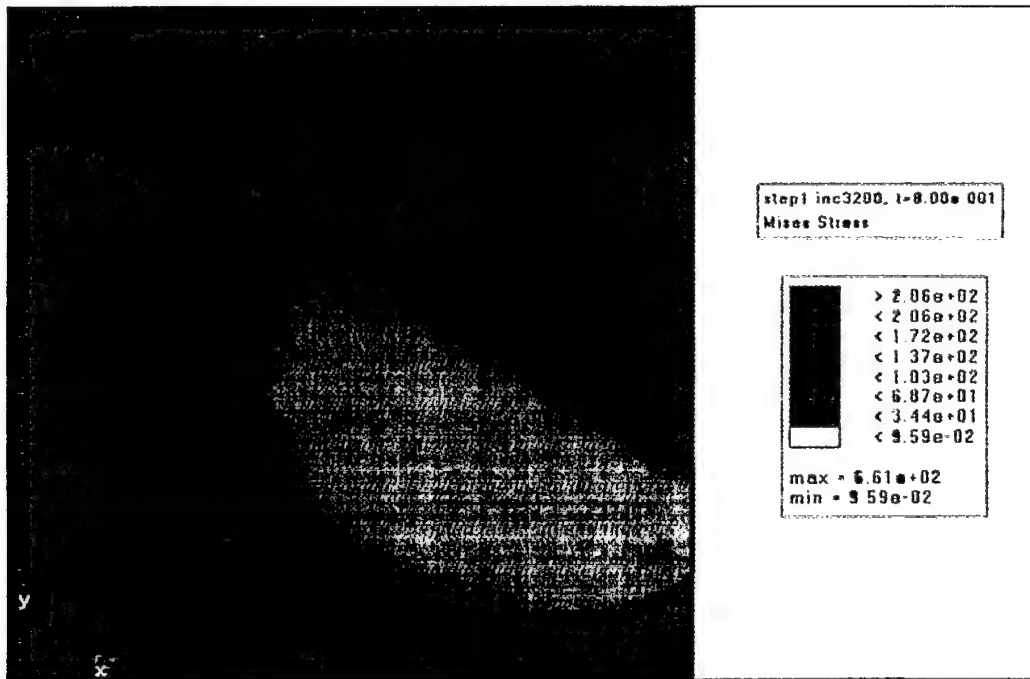
(e)



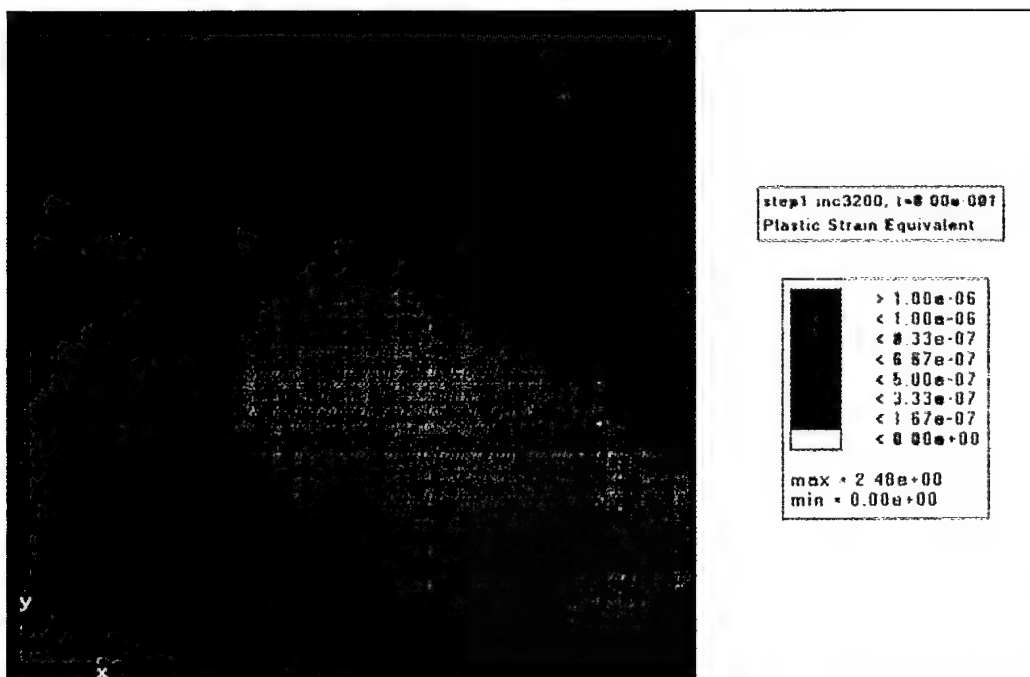
(f)

Figure 4.15 Continued: Plastic Zone Configurations of NS-304SS Specimens With Rising Stress-Strain Curve Model

(e) von Mises Stress and (f) Plastic Strain at 4.85 kN (0.74 P_L)



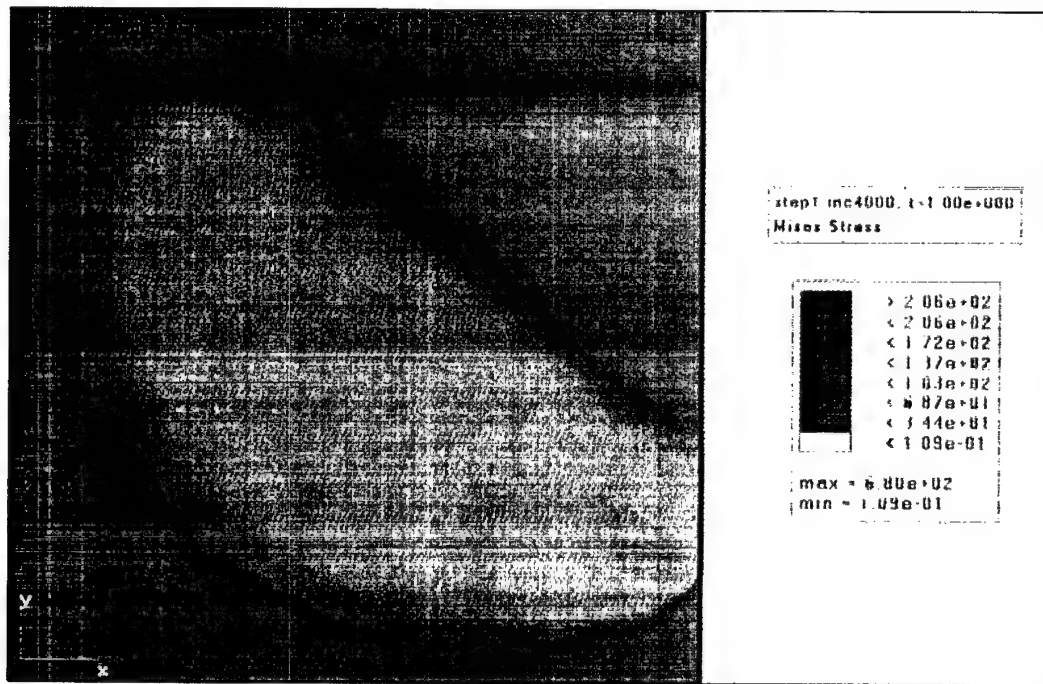
(g)



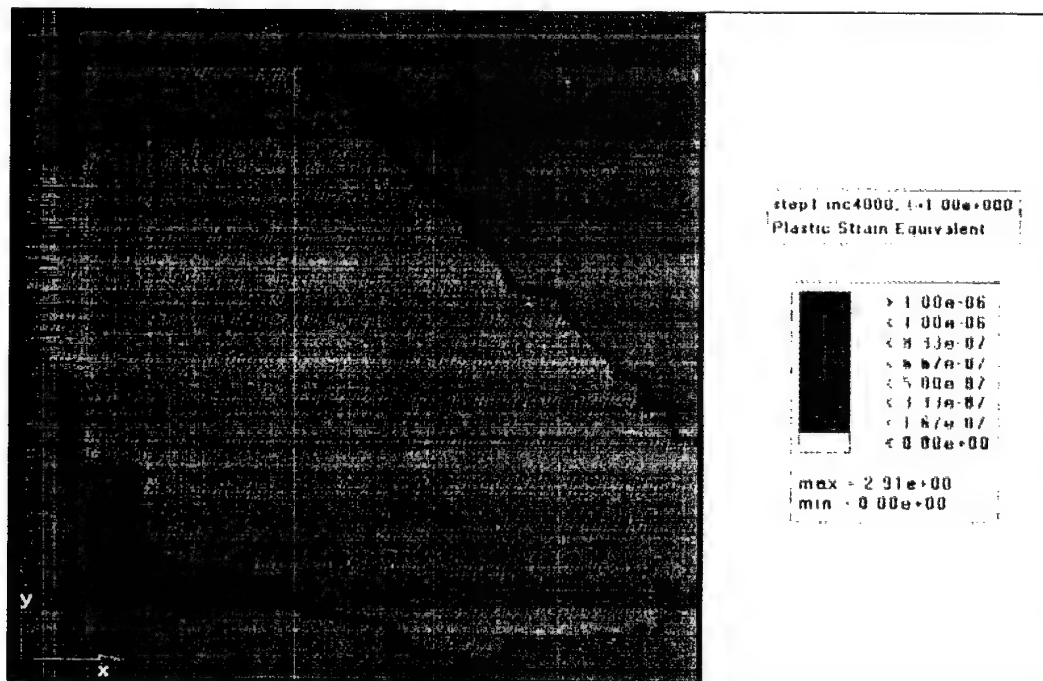
(h)

Figure 4.15 Continued: Plastic Zone Configurations of NS-304SS Specimens With Rising Stress-Strain Curve Model

(g) von Mises Stress and (h) Plastic Strain at 6.04 kN (0.92 P_L)



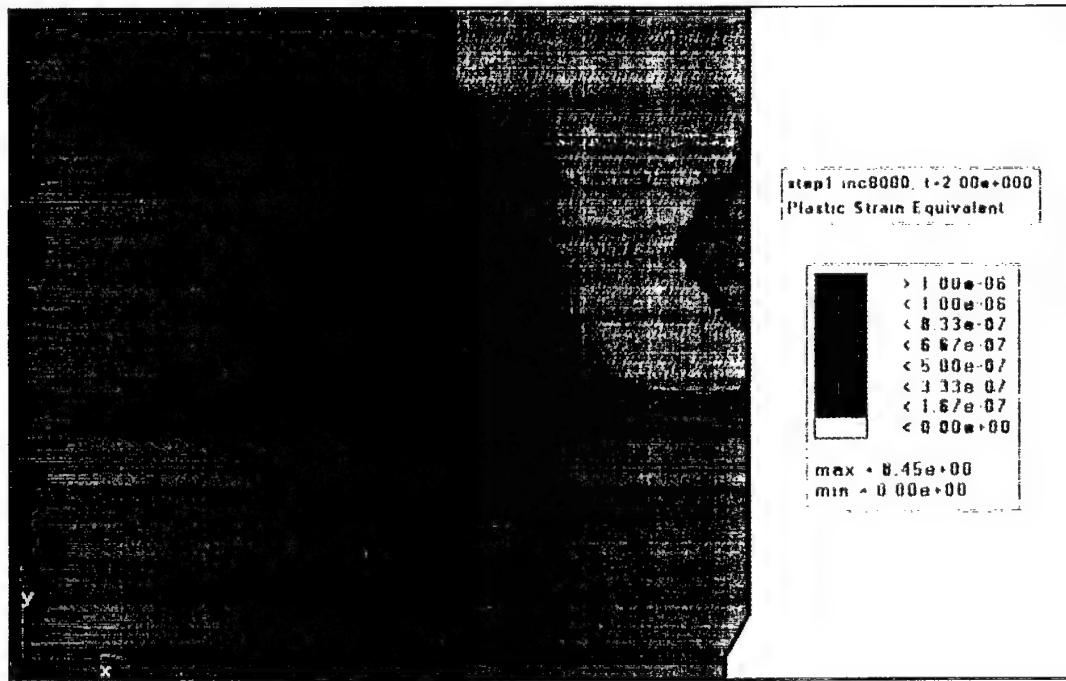
(i)



(j)

Figure 4.15 Continued: Plastic Zone Configurations of NS-304SS Specimens With Rising Stress-Strain Curve Model

(i) von Mises Stress and (j) Plastic Strain at 6.88 kN (1.04 P_L)



(k)

Figure 4.15 Continued: Plastic Zone Configurations of NS-304SS Specimens With Rising Stress-Strain Curve Model

(k) Plastic Strain at 7.79 kN (1.18 P_L)

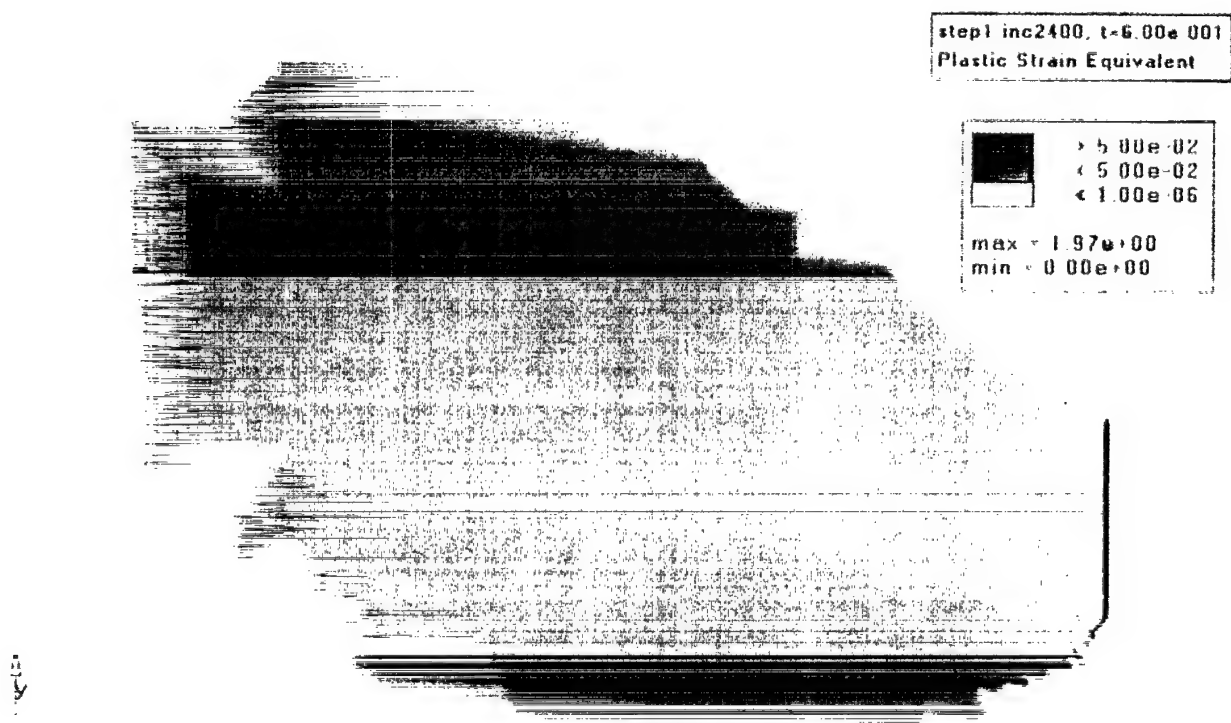


Figure 4.16: Plastic Zone Configuration of NS-304SS Specimen Showing Area With Greater Than 5% Plastic Strain at 4.85 kN (0.74 P_L)

5. SUMMARY, CONCLUSIONS AND RECOMMENDATIONS

5.1 Summary and Conclusions

This report focussed on a study to investigate plastic zone development in three point bend fracture specimen. The finite element methodology was utilized to provide an understanding of the plastic zone size (radius) to crack tip blunting (stretch zone width), in order to be able to predict the upper limit where elastic plastic fracture becomes invalid. Finite element analysis of three test specimen configurations were performed. The test specimens were (i) a standard dynamic tear (DT) test specimen with 350WT steel; (ii) another standard DT specimen with 304 stainless steel; and (iii) a non-standard three point bend specimen with 304 stainless steel. The ABAQUS finite element code was used to perform incremental elastic-plastic analysis of the specimens. Intuition and experimental observation were used to develop approximate stress-strain curves for the materials beyond the points where uniaxial stress-strain data were available for the 350WT steel and 304 stainless steel materials.

The results computed for each analysis included the midpoint displacement; development of the plastic zone around the crack tip with progression of load; the plastic zone radius r_p ; stretch zone width (SZW); and the ratio of plastic zone radius to SZW. The results were presented in the form of contour plots and charts for comparison with experiments being performed concurrently. It was found that the plastic zone radius r_p and stretch zone width SZW increased parabolically with load, up to $1.1 P_L$, where P_L is the limit load. On the other hand, the variation of the ratio r_p/SZW with load fitted a linear distribution for all cases. This ratio was found to vary from 50-90 for the DT specimen with 350WT steel; 140-150 for the DT specimen with 304 stainless steel and 90 -140 for the non-standard specimen with 304 stainless steel.

5.2 Recommendations

The experimental results were not fully available to this study, as they were being performed concurrently. It is recommended that the results of this study be compared to the

5.2

experimental results when they are available. Based on these comparisons it might be necessary to refine the stress-strain relations beyond the points where uniaxial test data available, to obtain better accuracy. Once a good level of accuracy has been achieved with the finite element model, it is further recommended that the analysis be applied to several other specimen configurations to enable a parameteric study to be performed. Such a study would lead to the generation of generalized charts that can be used for fracture measurements and design.

6. REFERENCES

- [1] Matthews, J.R. Porter, J.F. and Hyatt, C.V. "Fracture Control for Submarine Pressure Hulls II." 3rd Meeting of the TTCP PTP1 Operating Assignment on Fracture Control of Naval Structures, Annapolis, Maryland 1-3 May 1991.
- [2] Matthews, J.R., Porter, J.F., Hyatt, C.V. and KarisAllen, K.J. "A General Discussion of Short Crack Fracture." DREA Technical Paper.
- [3] Rice, J.R. in Journal of Applied Mechanics Series E of Transactions of the ASME, Vol., 90, June 1968.
- [4] Roy, V. Hyatt, C.V. and Matthews, J.R. "Precracking Stainless Steel 304 for Notch Tip Plastic Zone Studies." DREA Note No. DL(A)/98/1, 1998.
- [5] Hibbitt, H.D. Karlsson, B.I. and Sorensen, E.P. ABAQUS User's Manual, 1990.
- [6] DeGiorgi, V.G., Kirby III, G.C. and Jones, M.I. "Prediction of Classical Fracture Initiation Toughness." Engineering Fracture Mechanics, Vol. 33, No. 5, pp. 773-785, 1989.
- [7] DeGiorgi, V.G. and Matic, P. "A Computational Investigation of Local Material Strength and Toughness on Crack Growth." Engineering Fracture Mechanics, Vol. 39, No. 5, pp. 1039-1058, 1990.
- [8] DeGiorgi, V.G., Matic, P., Bar-on, I. and Lee, G.M.C. "An Experimental and Computational Investigation of Crack Growth Initiation in Three-Point Bend Fracture Specimens." Engineering Fracture Mechanics, Vol. 50, No. 1, pp. 1-9, 1995.
- [9] HyperMesh User's Manual.
- [10] Matthews, J.R. Private communications, 1999.
- [11] Boyer, H.E. Atlas of Stress-Strain Curves. ASM International, Metals Park, Ohio.

APPENDIX A

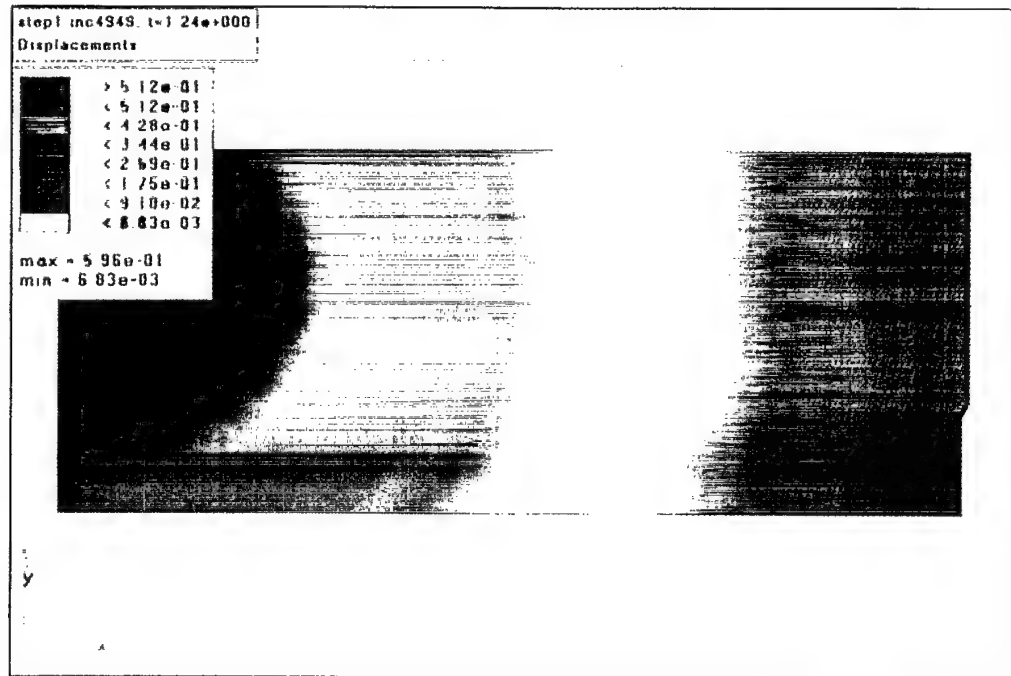
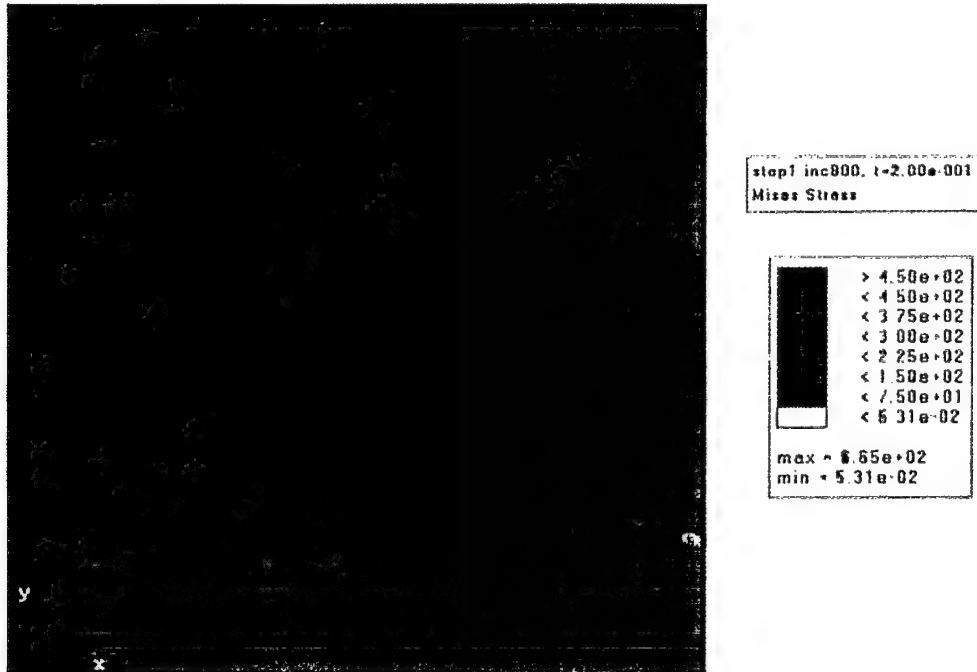
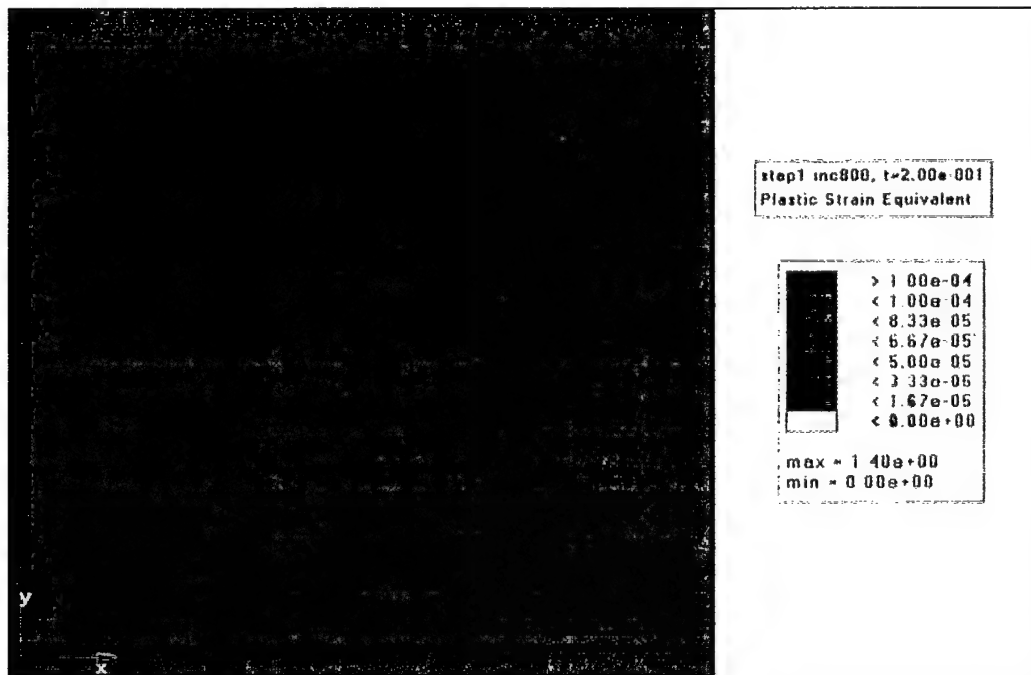


Figure A1: Displacement Contours of DT-350WT Specimen with Rising Stress-Strain Curve Model at $1.1P_L$



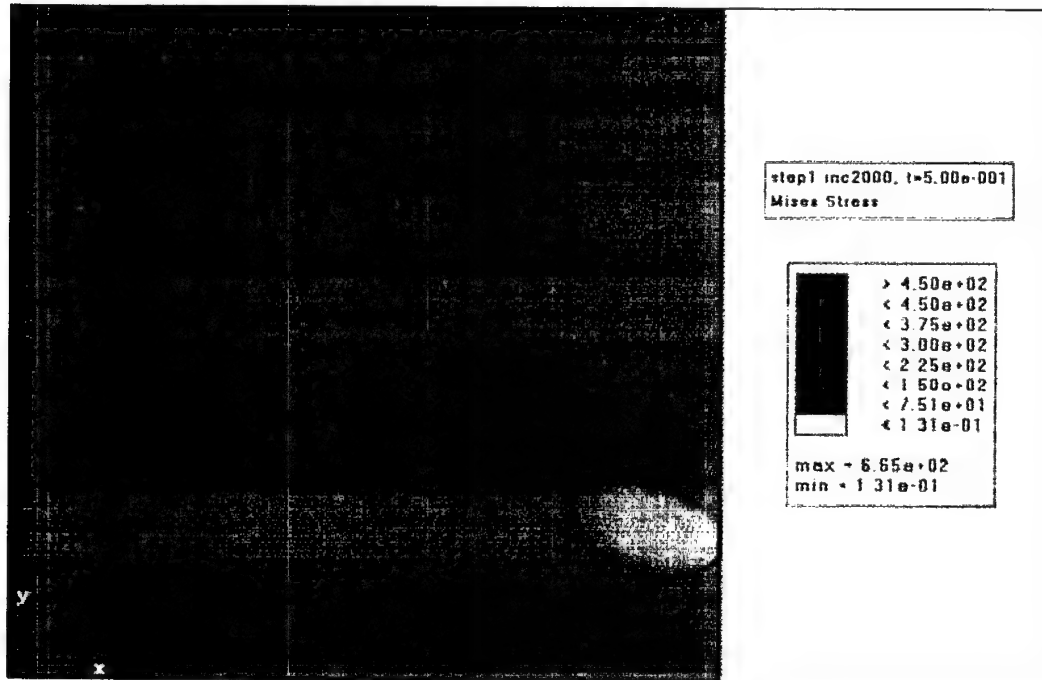
(a)



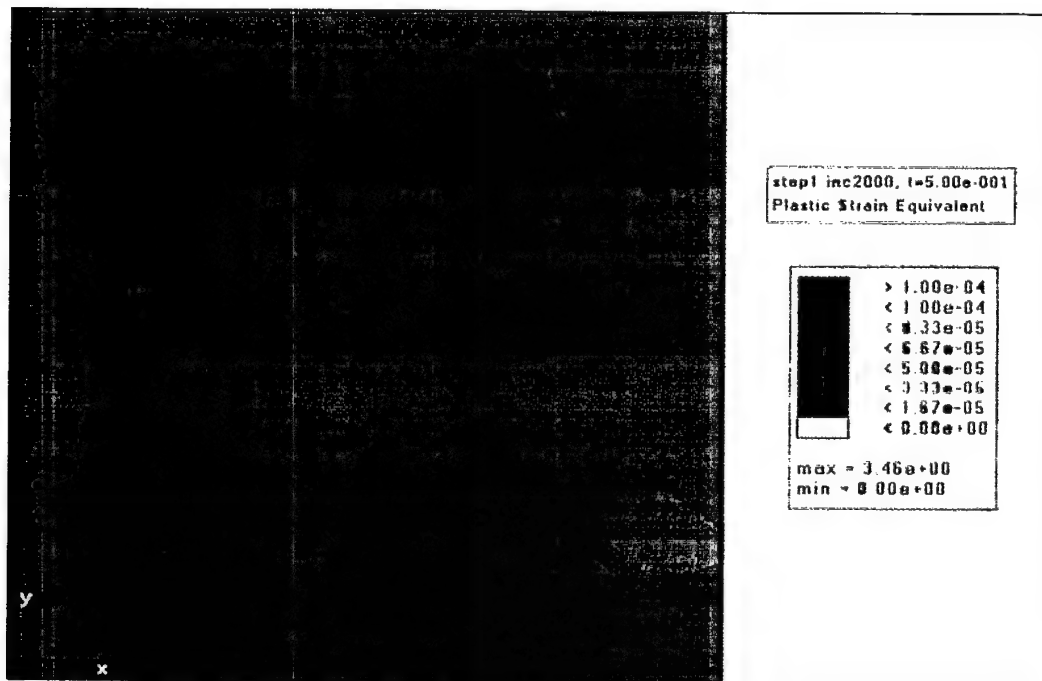
(b)

Figure A2: von Mises Stress and Equivalent Plastic Zone Development in DT-350WT Specimen with Flat Stress-Strain Curve Model

(a) von Mises Stress and (b) Plastic Strain at 3.19 kN (0.21 P_L)



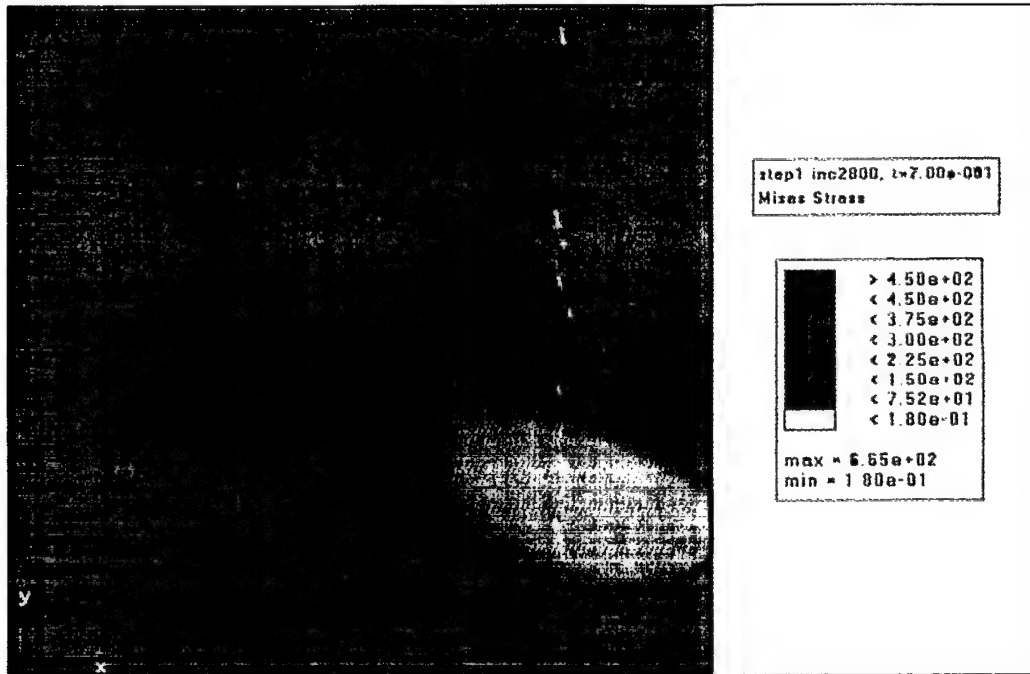
(c)



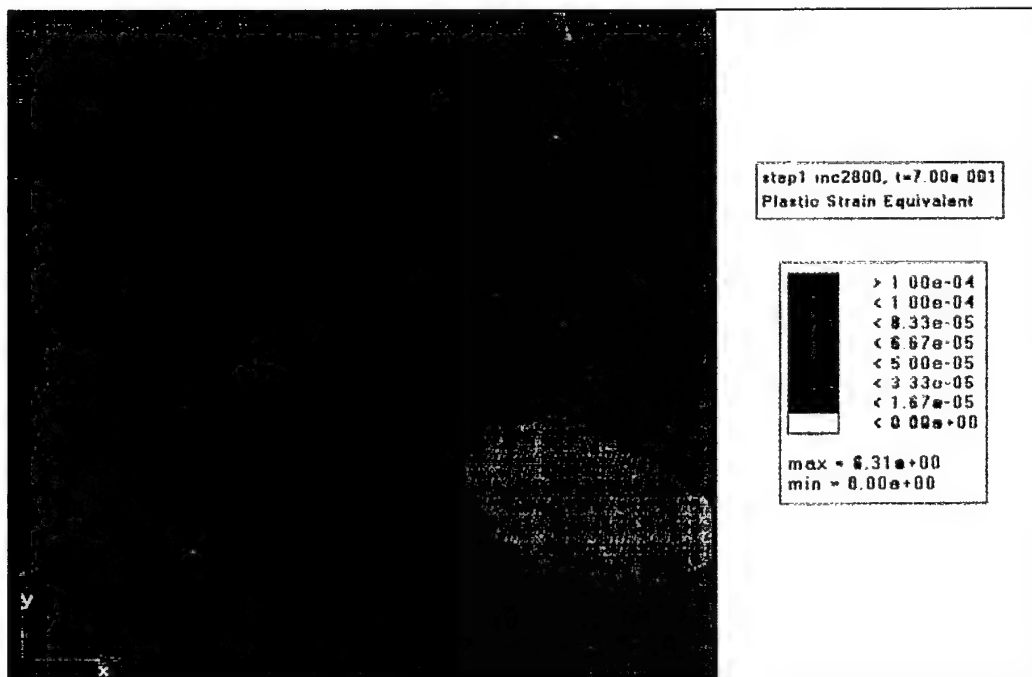
(d)

Figure A2 Continued: von Mises Stress and Equivalent Plastic Zone Development in DT-350WT Specimen with Flat Stress-Strain Curve Model

(c) von Mises Stress and (d) Plastic Strain at 7.87 kN (0.53 P_D)



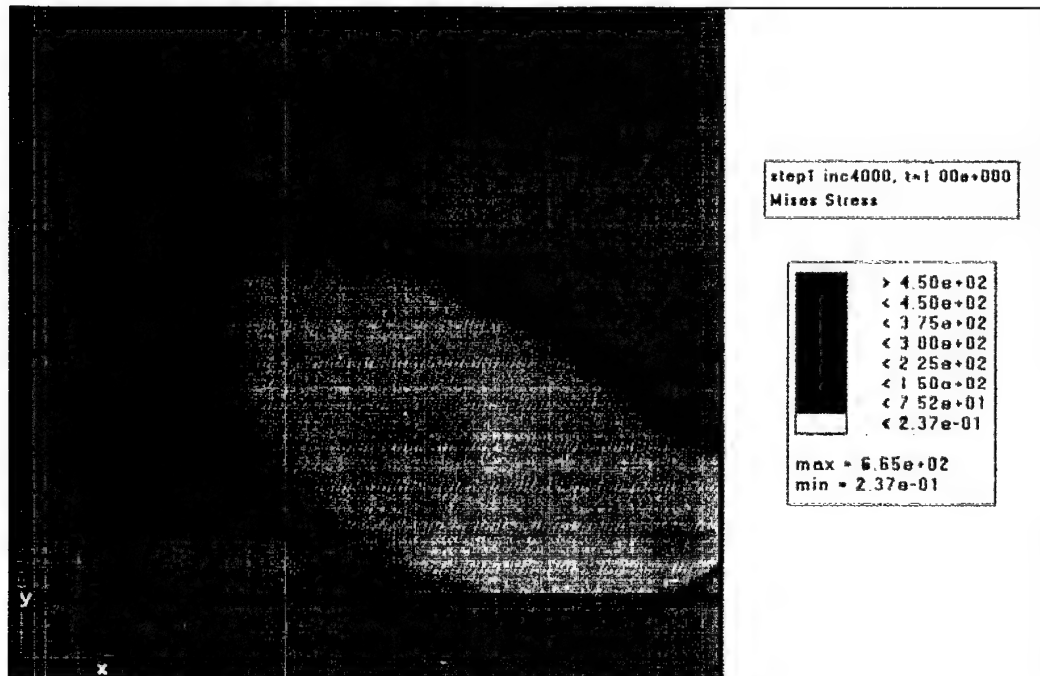
(e)



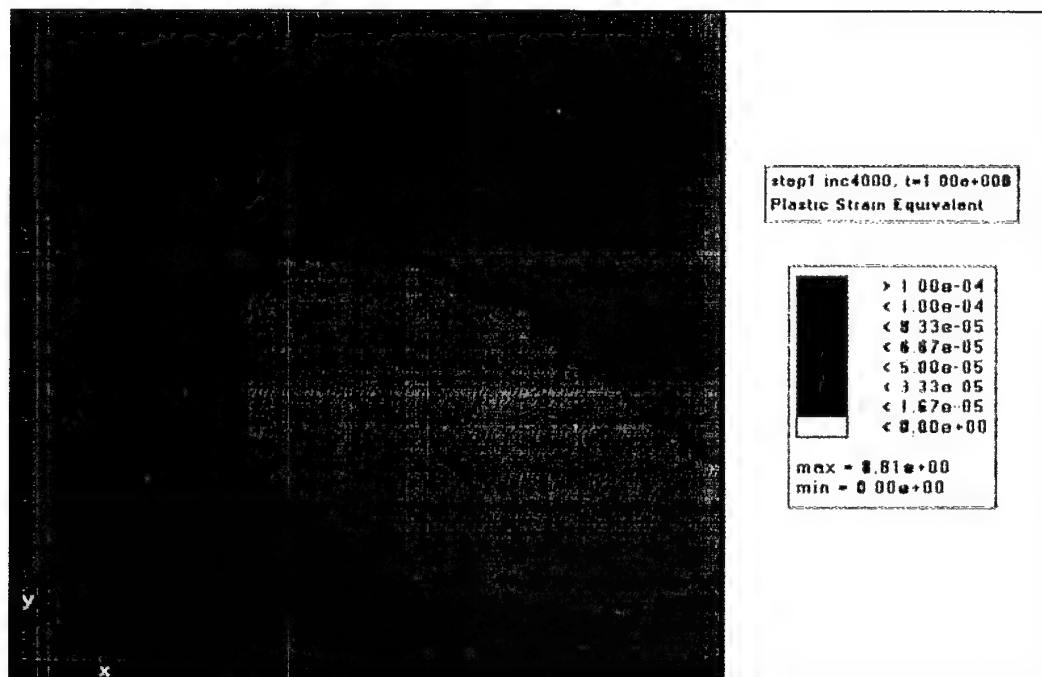
(f)

Figure A2 Continued: von Mises Stress and Equivalent Plastic Zone Development in DT-350WT Specimen with Flat Stress-Strain Curve Model

(e) von Mises Stress and (f) Plastic Strain at 10.81 kN (0.73 P_L)



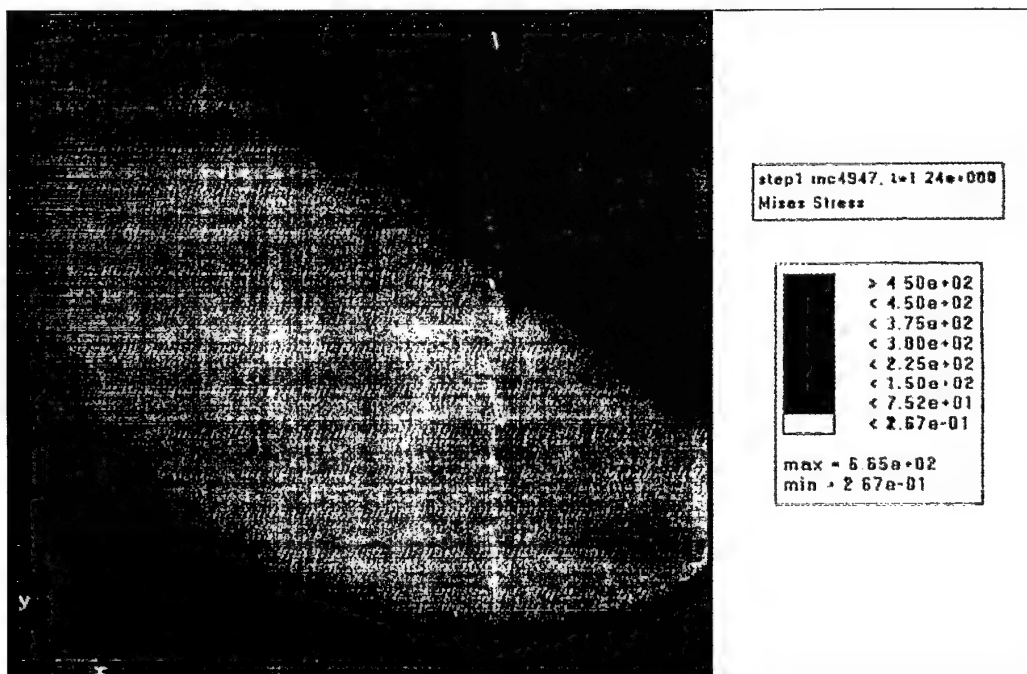
(g)



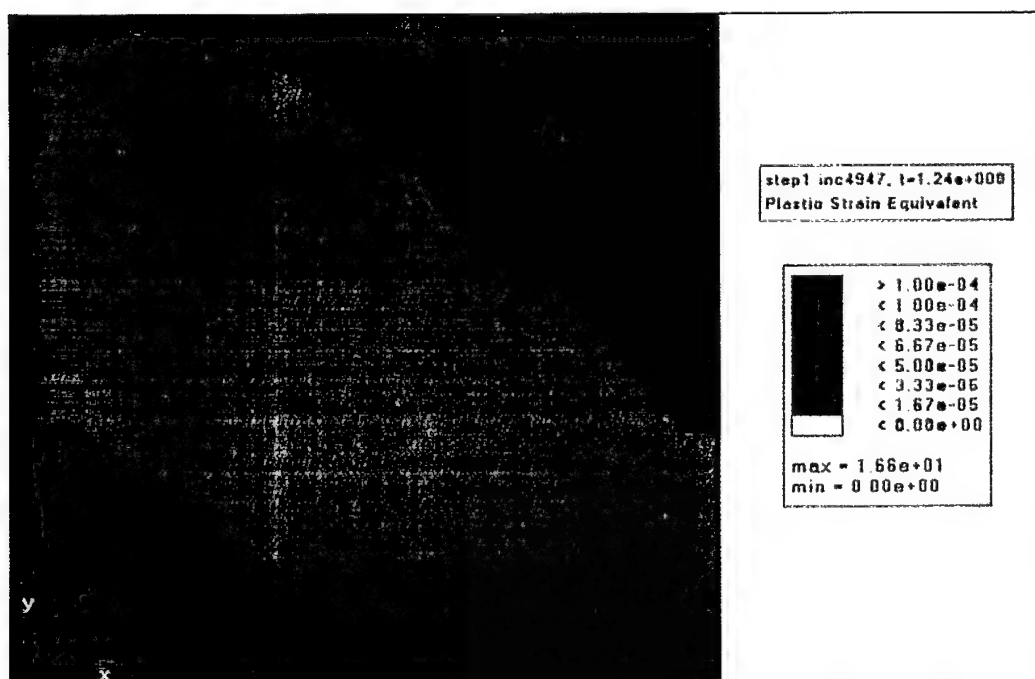
(h)

Figure A2 Continued: von Mises Stress and Equivalent Plastic Zone Development in DT-350WT Specimen with Flat Stress-Strain Curve Model

(g) von Mises Stress and (h) Plastic Strain at 14.24 kN (0.96 P_L)



(i)



(j)

Figure A2 Continued: von Mises Stress and Equivalent Plastic Zone Development in DT-350WT Specimen with Flat Stress-Strain Curve Model

(i) von Mises Stress and (j) Plastic Strain at 16.00 kN (1.08 P_L)

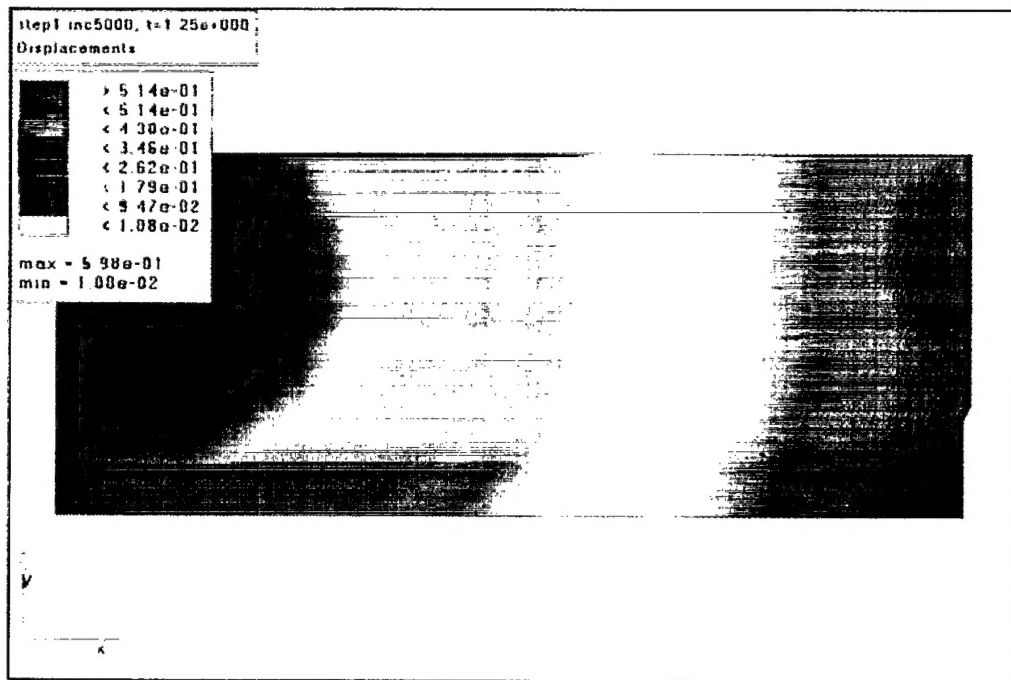


Figure A3: Displacement Contours of DT-304SS Specimen with Rising Stress Strain Curve Model at $1.044 P_L$

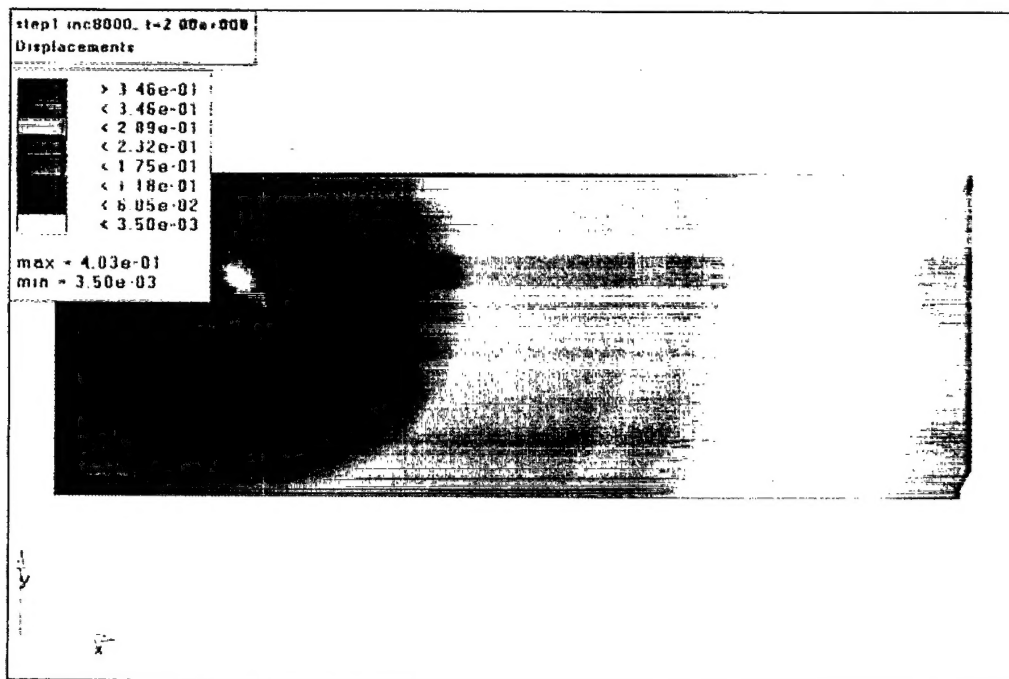


Figure A4: Displacement Contours of NS-304SS Specimen with Rising Stress-Strain Curve Model at $1.044 P_L$

UNCLASSIFIED
SECURITY CLASSIFICATION OF FORM
(highest classification of Title, Abstract, Keywords)

DOCUMENT CONTROL DATA		
(Security classification of title, body of abstract and indexing annotation must be entered when the overall document is classified)		
1. ORIGINATOR (the name and address of the organization preparing the document. Organizations for whom the document was prepared, e.g. Establishment sponsoring a contractor's report, or tasking agency, are entered in section 8.) Martec Limited 400-1888 Brunswick Street Halifax Nova Scotia Canada B3J 3J8	2. SECURITY CLASSIFICATION (overall security classification of the document including special warning terms if applicable). UNCLASSIFIED	
3. TITLE (the complete document title as indicated on the title page. Its classification should be indicated by the appropriate abbreviation (S,C,R or U) in parentheses after the title). Investigation of Plastic Zone Development in Dynamic Tear Test Specimens		
4. AUTHORS (Last name, first name, middle initial. If military, show rank, e.g. Doe, Maj. John E.) T.S. Koko, B.K. Gallant, S.M. Tobin		
5. DATE OF PUBLICATION (month and year of publication of document) July 1999	6a. NO. OF PAGES (total containing information Include Annexes, Appendices, etc.) 57 (approx.)	6b. NO. OF REFS (total cited in document) 11
7. DESCRIPTIVE NOTES (the category of the document, e.g. technical report, technical note or memorandum. If appropriate, enter the type of report, e.g. interim, progress, summary, annual or final. Give the inclusive dates when a specific reporting period is covered). CONTRACTOR REPORT		
8. SPONSORING ACTIVITY (the name of the department project office or laboratory sponsoring the research and development. Include address). Defence Research Establishment Atlantic PO Box 1012 Dartmouth, NS, Canada B2Y 3Z7		
9a. PROJECT OR GRANT NO. (if appropriate, the applicable research and development project or grant number under which the document was written. Please specify whether project or grant). Project 1GH36	9b. CONTRACT NO. (if appropriate, the applicable number under which the document was written). W7707-8-6180/A	
10a. ORIGINATOR'S DOCUMENT NUMBER (the official document number by which the document is identified by the originating activity. This number must be unique to this document.)	10b. OTHER DOCUMENT NOS. (Any other numbers which may be assigned this document either by the originator or by the sponsor.) DREA CR 1999-095	
11. DOCUMENT AVAILABILITY (any limitations on further dissemination of the document, other than those imposed by security classification) (X) Unlimited distribution () Defence departments and defence contractors; further distribution only as approved () Defence departments and Canadian defence contractors; further distribution only as approved () Government departments and agencies; further distribution only as approved () Defence departments; further distribution only as approved () Other (please specify):		
12. DOCUMENT ANNOUNCEMENT (any limitation to the bibliographic announcement of this document. This will normally correspond to the Document Availability (11). However, where further distribution (beyond the audience specified in (11) is possible, a wider announcement audience may be selected).		

UNCLASSIFIED
SECURITY CLASSIFICATION OF FORM

UNCLASSIFIED
SECURITY CLASSIFICATION OF FORM
(highest classification of Title, Abstract, Keywords)

13. **ABSTRACT** (a brief and factual summary of the document. It may also appear elsewhere in the body of the document itself. It is highly desirable that the abstract of classified documents be unclassified. Each paragraph of the abstract shall begin with an indication of the security classification of the information in the paragraph (unless the document itself is unclassified) represented as (S), (C), (R), or (U). It is not necessary to include here abstracts in both official languages unless the text is bilingual).

The J-Integral is an elastic-plastic fracture criterion, which permits measurement of the fracture toughness of a specimen that has been fractured after general yielding. However, an understanding of the ratio of plastic zone size (radius) to the crack tip blunting (stretch zone) required to determine the upper limit of temperature relative to full size transition curves where elastic plastic fracture becomes invalid. This study endeavours to acquire this ratio using finite element techniques.

The development of the plastic zone in dynamic tear (DT) specimens and a non- standard three point bending fracture test specimen used to measure fracture properties was the main focus of the study. The ABAQUS finite element software was used to model the elastic-plastic behaviour of the specimens. For the DT specimen, a crack was induced by pressing the notch, followed by fatigue cracking at a limit load level of 40% of the specimen limit load, whereas, the crack shape for the non-standard specimen was a fatigue crack defined at approximately 30% of the limit load. The shapes of these cracks were adequately modelled in the finite element analysis. The specimens were made of 350WT steel and 304 stainless steel materials. The specimens were loaded until fixed amounts of permanent deformation were recorded. Results were obtained in the form of plots, showing the progression of the plastic zone around the crack tip. For each case, the results provide the following: mid point plastic deflection, stretch zone width and plastic zone radius. The finite element results obtained were compared to experimental elastic plastic testing where available, and reasonably accurate agreement was achieved.

14. **KEYWORDS, DESCRIPTORS or IDENTIFIERS** (technically meaningful terms or short phrases that characterize a document and could be helpful in cataloguing the document. They should be selected so that no security classification is required. Identifiers, such as equipment model designation, trade name, military project code name, geographic location may also be included. If possible keywords should be selected from a published thesaurus. e.g. Thesaurus of Engineering and Scientific Terms (TEST) and that thesaurus-identified. If it not possible to select indexing terms which are Unclassified, the classification of each should be indicated as with the title).

Finite Element
Stretch Zone Width
Plastic zone radius
Transition Curves
Elastic Plastic Fracture Toughness
350WT plate steel
304 Stainless Steel

UNCLASSIFIED
SECURITY CLASSIFICATION OF FORM

The Defence Research
and Development Branch
provides Science and
Technology leadership
in the advancement and
maintenance of Canada's
defence capabilities.

Leader en sciences et
technologie de la défense,
la Direction de la recherche
et du développement pour
la défense contribue
à maintenir et à
accroître les compétences
du Canada dans
ce domaine.

512408



www.crad.dnd.ca